Natural gas-fired power plants valuation and optimisation under Lévy copulas and regime switching

Nemat Safarov
Imperial College London

Colin Atkinson
Imperial College London

December 16, 2016

Abstract

In this work we analyse a stochastic control problem for the valuation of a natural gas power station while taking into account operating characteristics. Both electricity and gas spot price processes exhibit mean-reverting spikes and Markov regime-switches. The Lévy regime-switching model incorporates the effects of demand-supply fluctuations in energy markets and abrupt economic disruptions or business cycles. We make use of skewed Lévy copulas to model the dependence risk of electricity and gas jumps. The corresponding coupled HJB equations are solved by an explicit finite difference method. The numerical approach gives us both the value of the plant and its optimal operating strategy depending on the gas and electricity prices, current temperature of the boiler and time. The surfaces of control strategies and contract values are obtained by implementing the numerical method for a particular example.

Keywords: power plant; stochastic control; coupled HJB equations; Lévy copulas, regime switching

2010 AMS Subject Classification: 35Q93; 0935R; 49M25; 60G51; 65C20

1 Introduction

The liberalisation of electricity and other energy markets, such as PJM in the United State, UKPX in the United Kingdom, Nord Pool in North Europe, and JEPX in Japan makes it necessary to incorporate highly volatile spot price dynamics into the optimisation problems for power generation.

During the traditional regulatory regime, the regulators used to set electricity prices based on cost of service. Investments in energy generating facilities

were allowed to earn a fixed return through electricity tariffs upon approval by the regulators. The economic viability of such investments and value of power plants could be calculated via a discounted cash flow (DCF) method. But it has been shown that the DCF approach doesn't give correct results as it ignores the opportunity costs (see Dixit & Pindyck 1994). Meanwhile, the existence of competitive electricity markets necessitates the valuation of power plants by means of financial instruments. This kind of real option approach to electricity generation was proposed by Deng et al. (2001). Deng & Oren (2003) further extend this work by including some physical operating constraints. Note that the omission of physical characteristics usually results in over-valuation.

The real options approach to power plant investment and optimisation problems has become an outstanding research area of different scientific groups. Pindyck (1993) applies this method to investigate the investment decisions to build a nuclear power plant. Tseng & Barz (2002) propose forward-moving Monte Carlo simulation with backward-moving dynamic programming technique to solve a multistage stochastic model used to evaluate a power plant with unit commitment constraints. Näsäkkälä & Fleten (2005) obtain a method to calculate thresholds for building a base load plant and upgrading it to a peak load plant when spark spread covers emission related costs. Takashima et al. (2007) investigate the investment problem for a power plant construction under the assumption that electricity prices are determined by the supply function and the equilibrium quantity.

Power generating assets can be classified as (a) nuclear, (b) hydroelectric, (c) fossil, or (d) renewable. In this work we will only consider fossil power stations. In general, a thermal power plant is a broader concept than fossil-fueled power generator. But we will use them interchangeably in this paper for simplicity purposes. Fossil power plants convert heat energy to electric power. More precisely, chemical energy in fossil fuels is first used to heat the water in the boiler. The resulting steam then spins the turbine which drives an electrical generator. The reader can refer to Wood & Wollenberg (2012) for more details regarding the operation of thermal power plants. Coal, natural gas and heating oil are the mostly used fuels for power generation. However, natural gas has become a primary fuel source for thermal power generators because of its low CO_2 emissions and flexibility during peak hours. The main objective in operating a power plant is to maximise the profit by utilising the difference (or spread) between electricity and natural gas prices. So, the valuation of a gas-fired power plant is closely related to spark spread, which is the most important cross-commodity transaction in power markets and is presented by Deng et al. (2001) as

$$S(t) = S_e(t) - cS_g(t), \tag{1}$$

where S_e and S_g are electricity and gas spot prices, respectively. heat rate is the amount of gas required to generate 1 MWh of electricity which is defined by heat rate c. It is a measure of efficiency. More precisely, the higher is the heat rate, the less efficient is the electricity generation. The heat rate has been usually assumed to be constant for convenience purposes (see Deng et al. 2001, Benth &

Kettler 2011, Meyer-Brandis & Morgan 2014). Deng & Oren (2003) generalise this approach by introducing an operating heat rate which changes depending on the discrete output levels. Thompson et al. (2004) consider the case where c is the amount of natural gas that needs to be burned to maximise the total revenue from electricity generation. In this model c depends continuously on time, boiler temperature, gas and electricity prices and is calculated via dynamic optimisation techniques.

The evaluation of a power plant cannot deliver satisfactory results without realistic stochastic models for underlying spot prices (see Fig 1). The detailed discussion of the related literature was presented in Safarov & Atkinson (2016). For completeness purposes we will briefly repeat them here.

A mean-reverting process is a common model for the energy spot price. For example, Schwartz (1997) presented three mean reverting models for commodity spot prices while assuming that stochastic convenience yield and interest rates also mean revert. Boogert & De Jong (2008) used the Least Square Monte Carlo method (initially proposed by Longstaff & Schwartz 2001 for American options) for gas storage valuation, while assuming the following one factor model for the spot price, which is calibrated to the initial futures curve:

$$\frac{dS(t)}{S(t)} = \kappa(\mu(t) - \ln S(t))dt + \sigma dB(t), \tag{2}$$

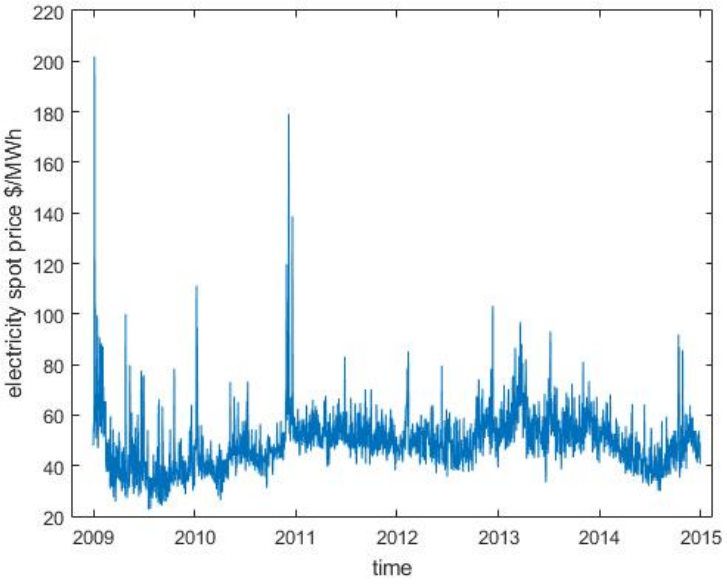
where B is a standard Brownian motion, μ is a time-dependent parameter, calibrated to the initial futures curve $(F(0,T))_{T\geq 0}$, provided by the market; the mean reversion parameter κ and the volatility σ are positive constants. One factor models are popular because of their simplicity. As is stated in Bjerksund et al. (2008), Henaff et al. (2013), it's unrealistic to assume that one factor models can capture all characteristics of highly volatile power or natural gas prices. Parsons (2013) extended equation (2) to the two-factor mean-reverting model where the long-term mean is also a mean-reverting process. Boogert & de Jong (2011) extended the application of the Least Square Monte Carlo method to multi-factor spot processes.

The unstorability of electricity in large quantities and storage complexities of natural gas create frequent demand-supply fluctuations in the corresponding commodity markets. These disruptions lead to the spiky behavior of energy spot prices. Therefore, price spikes have to be included in our spot price models as they carry out significant arbitrage opportunities.

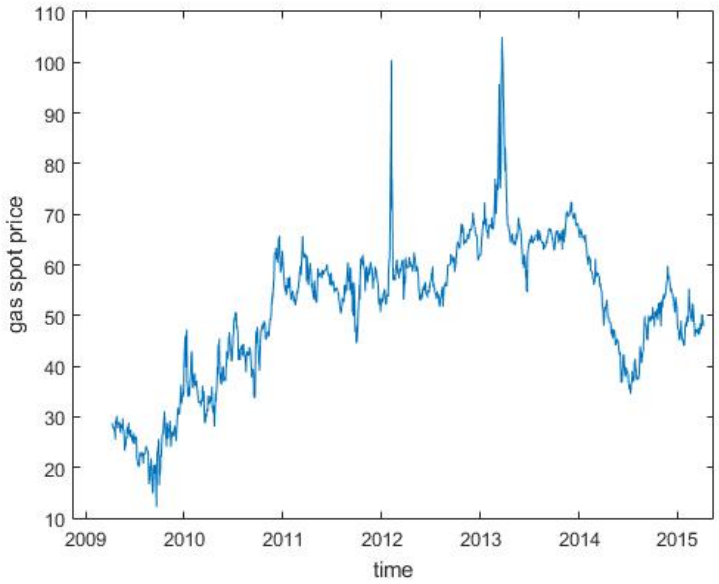
However, none of the models described above exhibit spiky instantaneous jumps of energy prices. Thompson et al. (2004, 2009) propose to model the risk adjusted power and natural spot prices, respectively by the following one dimensional continuous time Markov process:

$$dP = \mu_1(P,t)dt + \sigma_1(P,t)dX_1 + \sum_{k=1}^{N} \gamma_k(P,t,J_k)dq_k \tag{3}$$

where μ, σ, and the γ_k's are any arbitrary functions and the J_ks are arbitrary jump sizes with distributions $Q_k(J)$. X_1 and dq_k's denote the standard Brow-



(a) Electricity



(b) Natural gas

Figure 1: Day ahead UK spot prices for power and natural gas (NBP) during the time period 4 Sept 2009 - 4 July 2015 based on APX Power UK and Bloomberg.

nian motion and Poisson processes respectively. Eq. (3) covers a wide range of spot price models for natural gas and is tractable for numerical calculations. However, its jump component isn't appropriate to represent instant and mean-reverting spikes.

Benth et al. (2007) propose a more realistic alternative by defining energy spot dynamics as a sum of Ornstein-Uhlenbeck (OU) processes with different mean-reverting speeds. The only sources of randomness of the spot prices are positive pure jump processes. The additive structure of the model makes it difficult to derive futures curves. Therefore, Benth (2011) considers a stochastic volatility model by Barndorff-Nielsen & Shephard (2001) for equity markets in the context of energy commodities. Benth et al. (2013) generalise this non-Gaussian approach to a multivariate case to model the dynamics of cross-commodity spot prices.

The volatile behaviour of energy prices can differ significantly between cold and warm months. Benth et al. (2008) make use of time-inhomogeneous jump processes to capture these seasonality effects by introducing geometric and arithmetic spot price dynamics in the following way:

$$\ln S(t) = \ln \Lambda(t) + \sum_{i=1}^{m} X_i(t) + \sum_{j=1}^{n} Y_j(t), \qquad \text{(geometric)} \tag{4}$$

and

$$S(t) = \Lambda(t) + \sum_{i=1}^{m} X_i(t) + \sum_{j=1}^{n} Y_j(t), \qquad \text{(arithmetic)} \tag{5}$$

where

$$dX_i(t) = (\mu_i(t) - \alpha_i(t)X_i(t))dt + \sum_{k=1}^{p} \sigma_{ik}(t)dB_k(t), \tag{6}$$

$$dY_j(t) = (\delta_j(t) - \beta_j(t)Y_j(t))dt + \eta_j(t)dL_j(t), \tag{7}$$

for $i = 1, \ldots, m$ and $j = 1, \ldots, n$. Here B_k and L_j are independent standard Brownian motions and independent time-inhomogeneous Lévy processes, respectively. $\Lambda(t)$ is a deterministic, positive and continuously differentiable seasonality function, while the coefficients $\mu_i, \alpha_i, \delta_j, \beta_j, \eta_j$and σ_{ik} are continuous functions of t.

In Safarov & Atkinson (2016) the optimal operation problem for gas storage was investigated based on the geometric model. But for the optimisation of gas-fired power plant we will follow the arithmetic dynamics based on the justification presented in Benth et al. (2008), Meyer-Brandis & Morgan (2014).

Accurate valuation of power plants is impossible without the analysis of the multivariate dependence between electricity and gas prices. For Gaussian OU components it suffices to specify the appropriate covariance matrix. This

approach is not useful when we consider non-Gaussian spot price models. Therefore Meyer-Brandis & Morgan (2014) proposed to make use of Lévy copulas to model the dependence between the non-Gaussian OU components of electricity and gas spot prices. Although Thompson et al. (2004) develop a comprehensive stochastic control model which incorporates all the necessary operational constraints, the dependence of non-Gaussian jump components is assumed to be independent. In the actual calculations the gas prices are even assumed to be constant which is unlikely to be true under unregulated markets.

An alternative approach is the regime-switching framework initially proposed by Hamilton (1990). In a regime-switching model the price process can randomly shift between several regimes due to long-term demand-supply fluctuations, political instability, weather changes and other reasons. The spot price follows a distinct stochastic process within each regime. Carmona & Ludkovski (2010) and Chen & Forsyth (2010) apply a regime-switching approach to investigate stochastic control problems related to natural gas storage and implement the numerical calculation via Monte Carlo and finite difference methods, respectively. However, there is a lack of research related to the valuation of a power plant or spark-spread option under regime-switching models.

In this paper we investigate the valuation and optimal operation of gas-fired power generating facilities and refer to Thompson et al. (2004)for the physical operational constraints. But we assume that the underlying electricity and gas spot prices follow the Lévy regime-switching model. More precisely, at each regime the spot dynamics is defined by a special case of an arithmetic model (7). For the dependence of gas and electricity spikes we make use of skewed Lévy copulas for the reasons stated in Meyer-Brandis & Morgan (2014). Therefore, our approach not only incorporates the most important physical characteristics of a power plant but also takes into account short-term demand-supply variations and long-term economic disruptions.

We assume that the reader is familiar with fundamentals of the theory of Lévy processes, as presented for example in Cont & Tankov (2003), Schoutens (2003) and Kyprianou (2006).

To solve this stochastic control problem we employ the dynamic programming theory which gives us coupled Hamilton-Jacobi-Bellman (HJB) equations. We then solve this system of nonlinear partial integro-differential equations (PIDE) numerically.

2 Natural gas and electricity spot prices without regime switching

Let $(\Omega, \mathcal{F}, \{\mathcal{F}_t\}_{t\geq 0}, \mathbb{P})$ be a complete filtered probability space. We assume that the underlying spot prices follow the arithmetic model defined by eqs. (5) to (7). For simplicity, we take $m = n = p = 1$. We also define the initial condition

$$X(0) + Y(0) = S(0) - \Lambda(0). \tag{8}$$

Then we have the following dynamics for $S(t)$:

$$S(t) = \Lambda(t) + X(t) + Y(t), \tag{9}$$

where

$$dX(t) = (\mu(t) - \alpha(t)X(t))dt + \sigma(t)dB(t), \tag{10}$$
$$dY(t) = (\delta(t) - \beta(t)Y(t))dt + \eta(t)dL(t), \tag{11}$$

We further assume that the coefficients of eqs. (10) and(11) are constants such that $\mu(t) = \delta(t) = 0, \alpha(t) = \beta(t) = \alpha^e, \sigma(t) = \sigma$ and $\eta(t) = 1$. Then the dynamics of electricity spot prices is given by

$$S^e(t) = \Lambda_e(t) + X^e(t) + Y^e(t), \tag{12}$$

where

$$dX^e(t) = -\alpha_e X^e(t)dt + \sigma_e dB^e(t), \tag{13}$$
$$dY^e(t) = -\alpha_e Y^e(t)dt + dL^e(t), \tag{14}$$

The underlying natural gas spot price follows the similar model:

$$S^g(t) = \Lambda_g(t) + X^g(t) + Y^g(t), \tag{15}$$

where

$$dX^g(t) = -\alpha_g X^g(t)dt + \sigma_g dB^g(t), \tag{16}$$
$$dY^g(t) = -\alpha_g Y^g(t)dt + dL^g(t). \tag{17}$$

Note that we could take unequal mean-reversion rates for normal variations and jumps in our spot price models following Safarov & Atkinson (2016). But that would increase the dimension of our HJB equation which is derived in section 3. We keep them equal to reduce the computational time.

In general, L^e and L^g can be subordinator Lévy processes

$$L^e(t) = \int_0^t \int_{\mathbb{R}_+} zJ^e(dz, ds) \qquad \text{and} \qquad L^g(t) = \int_0^t \int_{\mathbb{R}+} zJ^g(dz, ds) \tag{18}$$

where $J^e(dz, ds)$ and $J^g(dz, ds)$ are Poisson random measures with the corresponding Lévy intensity measures $\nu^e(dz, ds)$ and $\nu^g(dz, ds)$ (see Jacod & Shiryaev (2013)). These jump measures have positive supports because we only consider upward price spikes. Following Meyer-Brandis & Morgan (2014) we further assume that L^e and L^g are compound Poisson processes with intensities λ_e and λ_g and jump size distributions D_e and D_g, respectively. In other words,

$$\nu^e(dz, ds) = \lambda_e D_e(dz)ds = \nu^e(dz)ds, \tag{19}$$
$$\nu^g(dz, ds) = \lambda_g D_g(dz)ds = \nu^g(dz)ds. \tag{20}$$

The complete characterisation of the two-dimensional model $(S^e(t), S^g(t))$ requires the specification of the dependence risk between the spot prices S^e and S^g. We can separate this problem in defining the multivariate distributions of $(B^e(t), B^g(t))$ and $(L^e(t), L^g(t))$. The former issue can be easily resolved by determining the correlation parameter ρ between $B^e(1)$ and $B^g(1)$

$$dB^e(t)dB^g(t) = \rho dt. \tag{21}$$

To specify the dependence between power and gas spot prices we will refer to Meyer-Brandis & Morgan (2014) for using positive Lévy copulas. This concept will be analysed in section 4.

Before moving to the optimisation problem of a power plant we can write the electricity and gas spot price models in a more convenient SDE form as follows:

$$\begin{aligned} dS^e(t) &= d\Lambda_e(t) + dX^e(t) + dY^e(t), \\ &= \Lambda_e'(t)dt - \alpha_e(X^e(t) + Y^e(t))dt + \sigma_e dB^e(t) + dL^e(t) \\ &= \Lambda_e'(t)dt - \alpha_e(S^e(t) - \Lambda_e(t))dt + \sigma_e dB^e(t) + dL^e(t) \\ &= (\bar{\Lambda}_e(t) - \alpha_e S^e(t))dt + \sigma_e dB^e(t) + dL^e(t) \end{aligned} \tag{22}$$

where $\bar{\Lambda}_e(t) = \Lambda_e'(t) + \alpha^e \Lambda_e(t)$ Similarly, we can derive the SDE for the gas spot price

$$dS^g(t) = (\bar{\Lambda}_g(t) - \alpha_g S^g(t))dt + \sigma_g dB^g(t) + dL^g(t) \tag{23}$$

Note that we can get the compensated compound Poisson processes $\tilde{L}^e(t)$ and $\tilde{L}^g(t)$ as follows:

$$\tilde{L}^e(t) = \int_0^t \int_{\mathbb{R}+} z(J^e(dz, ds) - \nu^e(dz, ds)) = \int_0^t \int_{\mathbb{R}_+} z\tilde{J}^e(dz, ds) \tag{24}$$

$$\tilde{L}^g(t) = \int_0^t \int_{\mathbb{R}+} z(J^g(dz, ds) - \nu^g(dz, ds)) = \int_0^t \int_{\mathbb{R}_+} z\tilde{J}^g(dz, ds) \tag{25}$$

where $\tilde{J}^e$ and $\tilde{J}^g$ are compensated Poisson random measures. Then eqs. (22) and (23) transform to

$$dS^e(t) = (\tilde{\Lambda}_e(t) - \alpha_e S^e(t))dt + \sigma_e dB^e(t) + \int_{\mathbb{R}_+} z\tilde{J}^e(dz, dt) \tag{26}$$

$$dS^g(t) = (\tilde{\Lambda}_g(t) - \alpha_g S^g(t))dt + \sigma_g dB^g(t) + \int_{\mathbb{R}_+} z\tilde{J}^e(dz, dt). \tag{27}$$

where $\tilde{\Lambda}_e(t) = \bar{\Lambda}_e(t) + \int_{\mathbb{R}_+} z\nu^e(dz)$ and $\tilde{\Lambda}_g(t) = \bar{\Lambda}_g(t) + \int_{\mathbb{R}_+} z\nu^g(dz)$.

3 Optimal control of power generation

The theoretical framework and physical constraints for the optimal operation of a gas-fired power generator will be based on Thompson et al. (2004). Therefore, the following physical characteristics need to be incorporated in our optimisation model:

(i) The minimum generation temperature: The plant cannot operate below a certain temperature.

(ii) Variable start-up times: The time required to heat the boiler to its minimum generation level depends on the heat rate of natural gas and the current temperature.

(iii) The variable output rates: The efficiency of the plant varies non-linearly with the amount of generated electricity.

(iv) The variable start-up and production costs. Increase of electricity output is achieved by raising the boiler temperature. The fuel used for this heat increase does not generate any additional power.

(v) Control response time lags: Changing boiler temperature takes some time. Therefore, any decision to alter the power output will take effect after a reasonable amount of time.

(vi) The ramp rate limit: This is the minimum amount of time required for switching a unit on/off to avoid thermal stress and fatigue.

Following Thompson et al. (2004) we model the boiler temperature L as a state variable and incorporate all these operational constraints in its mean-reverting equation

$$dL = \eta(L, c)(\bar{L}(c) - L)dt \tag{28}$$

where c is the variable controlling the amount of gas consumed per instant in time; $\bar{L}(c)$ is the equilibrium temperature of the generator depending on c; η is a mean-reverting speed function specific to each power plant.

The non-linear dependence of the amount of produced electricity on the boiler temperature is given by the output function $H(L)$. We can now move to our stochastic control problem for the power plant.

The objective of the optimisation is to find a control variable $c(S_e, S_g, L, t)$ that maximises the expected future cash flow up to maturity time T and discounted at a rate r

$$V(S_e, S_g, L, t) = \max_{c(S_e, S_g, L, t)} \mathbb{E}\left[\int_t^T e^{-r(\tau - t)}(H(L)S_e - S_g c)d\tau\right], \tag{29}$$

subject to

$$c_{min}(L) \leq c \leq c_{max}(L). \tag{30}$$

The minimum and maximum bounds on c are necessary to avoid thermal stresses.

Rewriting (29) in a similar way to Thompson et al. (2004) will lead to the Bellman equation:

$$\begin{aligned} V &= \max_c \mathbb{E}\left[\int_t^{t+dt} e^{-r(\tau-t)}(H(L)S_e - S_g c)d\tau + \int_{t+dt}^{T} e^{-r(\tau-t)}(H(L)S_e - S_g c)d\tau\right] \\ &= \max_c \mathbb{E}\left[\int_t^{t+dt} e^{-r(\tau-t)}(H(L)S_e - S_g c)d\tau + e^{-rdt}\int_{t+dt}^{T} e^{-\rho(\tau-(t+dt))}(H(L)S_e - S_g c)d\tau\right] \\ &= \max_c \mathbb{E}\left[\int_t^{t+dt} e^{-r(\tau-t)}(H(L)S_e - S_g c)d\tau + e^{-rdt}V(S_e + dS_e, S_g + dS_g, L + dL, t + dt)\right]. \end{aligned} \tag{31}$$

We can now apply the multidimensional Itô's formula (see Cont & Tankov (2003)) to $V(S_e, S_g, L, t)$ to expand it above in Taylor's series:

$$\begin{aligned} V = \max_c \mathbb{E}[&(H(L)S_e - S_g c)dt + (1 - rdt)[V + V_t dt + V_L dL \\ &+ V_{S_e}dS_e + V_{S_g}dS_g + \frac{1}{2}V_{S_eS_e}d[S_e, S_e]_t^c + \frac{1}{2}V_{S_gS_g}d[S_g, S_g]_t^c + V_{S_eS_g}d[S_e, S_g]_t^c \\ &+ \iint_{\mathbb{R}^2_+}(V(S_e + z_e, S_g + z_g, L, t) - V(S_e, S_g, L, t) - z_e V_{S_e} - z_g V_{S_g})J(dz, dt)], \end{aligned} \tag{32}$$

where $J(dz, dt) = J(dz_e, dz_g, dt)$ is a two-dimensional Poisson random measure with Lévy intensity measure $\nu(dz, dt)$ and

$$d[S_e, S_e]_t^c = \sigma_e^2 dt, \quad d[S_g, S_g]_t^c = \sigma_g^2 dt \quad \text{and} \quad d[S_e, S_g]_t^c = \rho\sigma_e\sigma_g dt. \tag{33}$$

We then denote

$$\mu_e(S^e, t) = \tilde{\Lambda}_e(t) - \alpha_e S^e(t) \tag{34}$$

and

$$\mu_g(S^g, t) = \tilde{\Lambda}_g(t) - \alpha_g S^g(t) \tag{35}$$

for clarity purposes. After substituting eqs. (26) to (28) and (33) in equation (32) we obtain

$$\begin{aligned} V = \max_c \mathbb{E}[&(H(L)S_e - S_g c)dt + (1 - rdt)(V + V_t + \\ &\eta(L, c)(\bar{L}(c) - L)V_L + \mu_e(S^e, t)V_{S_e} + \mu_g(S^g, t)V_{S_g} + \\ &\frac{1}{2}\sigma_e^2 V_{S_eS_e} + \frac{1}{2}\sigma_g^2 V_{S_gS_g} + \rho\sigma_e\sigma_g V_{S_eS_g})dt + \sigma_e dB^e(t) + \sigma_g dB^g(t) \\ &\iint_{\mathbb{R}^2_+}(V(S_e + z_e, S_g + z_g, L, t) - V(S_e, S_g, L, t) - z_e V_{S_e} - z_g V_{S_g})\nu(dz, dt) + \\ &\iint_{\mathbb{R}^2_+}(V(S_e + z_e, S_g + z_g, L, t) - V(S_e, S_g, L, t))\tilde{J}(dz, dt))], \end{aligned} \tag{36}$$

Elimination of all terms that go to zero faster than dt and some further simplifications similar to Safarov & Atkinson (2016) results in the following HJB equation

$$\max_c [V_t + \frac{1}{2}\sigma_e^2 V_{S_e S_e} + \frac{1}{2}\sigma_g^2 V_{S_g S_g} + \rho\sigma_e\sigma_g V_{S_e S_g} + \mu_e(S^e, t)V_{S_e} + \mu_g(S^g, t)V_{S_g} - rV + \iint_{\mathbb{R}^2_+} (V(S_e + z_e, S_g + z_g, L, t) - V(S_e, S_g, L, t) - z_e V_{S_e} - z_g V_{S_g})\nu(dz, dt) + H(L)S_e - S_g c + \eta(L, c)(\bar{L}(c) - L)V_L] = 0 \quad (37)$$

Note that the control variable c only appears in the last two terms. We also need to introduce time to maturity $\tau = T - t$. Then HJB equation above becomes

$$V_\tau = \frac{1}{2}\sigma_e^2 V_{S_e S_e} + \frac{1}{2}\sigma_g^2 V_{S_g S_g} + \rho\sigma_e\sigma_g V_{S_e S_g} + \mu_e(S^e, T-\tau)V_{S_e} + \mu_g(S^g, T-\tau)V_{S_g} - rV + \iint_{\mathbb{R}^2_+} (V(S_e + z_e, S_g + z_g, L, \tau) - V(S_e, S_g, L, \tau) - z_e V_{S_e} - z_g V_{S_g})\nu(dz, d\tau) + \max_c [H(L)S_e - S_g c + \eta(L, c)(\bar{L}(c) - L)V_L] = 0 \quad (38)$$

where

$$c_{min}(L) \leq c \leq c_{max}(L). \quad (39)$$

In other words, the maximisation problem reduces to

$$c^*(S_e, S_g, L, \tau) = \arg\max_c [H(L)S_e - S_g c + \eta(L, c)(\bar{L}(c) - L)V_L] \quad (40)$$

After the calculation of the optimal strategy c^* we substitute it in equation (38) to get

$$V_\tau = \frac{1}{2}\sigma_e^2 V_{S_e S_e} + \frac{1}{2}\sigma_g^2 V_{S_g S_g} + \rho\sigma_e\sigma_g V_{S_e S_g} + \mu_e(S^e, T-\tau)V_{S_e} + \mu_g(S^g, T-\tau)V_{S_g} - rV + \iint_{\mathbb{R}^2_+} (V(S_e + z_e, S_g + z_g, L, \tau) - V(S_e, S_g, L, \tau) - z_e V_{S_e} - z_g V_{S_g})\nu(dz, d\tau) + H(L)S_e - S_g c^* + \eta(L, c^*)(\bar{L}(c^*) - L)V_L] \quad (41)$$

Thus, once the optimal control c^* is known, the nonlinear HJB equation simplifies to linear PIDE. Before starting our numerical approach to solve equation (41), we analyse the two-dimensional Lévy measure ν by means of Lévy copulas in the next section.

4 Lévy copula

Before starting the analysis of the dependence of $(L^e(t), L^g(t))$ we need to go through some brief introduction on Lévy copulas. We will refer to Cont & Tankov (2003), Kallsen & Tankov (2006) for the detailed background on this concept. We will mainly use the following key results in our investigation:

Theorem 4.1 *(Sklar's Theorem for Lévy copulas) Let $(X(t), Y(t))$ be a two-dimensional Lévy process with positive jumps that have tail integral $U(x, y)$ and marginal tail integrals $U_1(x)$ and $U_2(y)$. Then there exists a unique positive Lévy copula F such that:*

$$U(x, y) = F(U_1(x), U_2(y)), \quad \forall x, y \in [0, \infty). \tag{42}$$

Conversely, if F is a positive Lévy copula, $X(t)$ and $Y(t)$ are one-dimensional Lévy processes with tail integrals U_1,U_2 then there exists a two-dimensional Lévy process such that its tail integral is given by equation (42)*.*

An Archimedean Lévy copula is a popular parametric Lévy copula defined as

$$F(x, y) = \phi^{-1}(\phi(x) + \phi(y)), \tag{43}$$

where ϕ is a strictly decreasing convex function with positive support such that $\phi(0) = \infty$ and $\phi(\infty) = 0$. In these models F is always assumed to have the symmetry property $F(x, y) = F(y, x)$. However Meyer-Brandis & Morgan (2014) argue that this symmetry property is not supported by the data. Therefore they introduce skewed Archimedean Lévy copulas as follows

$$F(x, y) = \phi^{-1}(\psi_1(y)\phi(x) + \psi_2(x)\phi(y)), \tag{44}$$

where ψ_1 and ψ_2 are decreasing functions satisfying $\psi_1(\infty) = \psi_2(\infty) = 1$, while ϕ is the same as above. In our calculations we will use the skewed Clayton-Lévy copula where

$$\phi(x) = x^{-\theta}, \quad \psi_1(x) = (\alpha x^{-\beta} + 1), \quad \textit{and} \quad \psi_2 \equiv 1, \tag{45}$$

for $\alpha > 0, \theta > 0$ and $0 < \beta \leq \theta + 1$. More precisely,

$$F(x, y) = ((\alpha y^{-\beta} + 1)x^{-\theta} + y^{-\theta})^{-1/\theta} \tag{46}$$

We can construct multivariate jump densities from univariate ones by using Lévy copulas. The following is the two-dimensional version of the Lemma proposed by Reich et al. (2010).

Lemma 4.2 *Let $f \in C^2(\mathbb{R}^2)$ be a bounded function vanishing on a neighbourhood of the origin. Moreover, let $(X(t), Y(t))$ be a two-dimensional Lévy process with Lévy measure ν, Lévy copula F, and marginal Lévy measures ν_1 and ν_2. Then*

$$\begin{aligned}\int_{\mathbb{R}^2} f(x, y)\nu(dx, dy) = &\int_{\mathbb{R}} \frac{\partial f}{\partial x}(x, 0)\nu_1(dx) + \int_{\mathbb{R}} \frac{\partial f}{\partial y}(0, y)\nu_2(dy) \\ &+ \int_{\mathbb{R}^2} \frac{\partial^2 f}{\partial x \partial y}(x, y)F(U_1(x), U_2(y))dxdy.\end{aligned} \tag{47}$$

We can now make use of this Lévy copula techniques to break the double integral term in equation (41) into parts that can be calculated via standard numerical

integration techniques. First of all, let's denote the integrand as follows to reduce the size of calculations

$$G(z_e, z_g) = V(S_e + z_e, S_g + z_g, L, \tau) - V(S_e, S_g, L, \tau) - z_e V_{S_e} - z_g V_{S_g} \quad (48)$$

for fixed $S = (S_e, S_g)$ and L. The application of Lemma 4.2 to the integral term in equation (41) results in

$$\int_{\mathbb{R}^2_+} G(z_e, z_g)\nu((dz_e \times dz_g) = \int_{\mathbb{R}_+} \frac{\partial G}{\partial z_e}(z_e, 0)\nu_1((dz_e) + \int_{\mathbb{R}_+} \frac{\partial G}{\partial z_g}(0, z_g)\nu_2(dz_g) + \int_{\mathbb{R}^2_+} \frac{\partial^2 G}{\partial z_e \partial z_g}(z_e, z_g)F(U_1(z_e), U_2(z_g))dz_e dz_g. \quad (49)$$

By taking the partial derivatives of G in equation (48) we obtain

$$\begin{aligned} \frac{\partial G}{\partial z_e}(z_e, 0) &= V_{S_e}(S_e + z_e, S_g, L, \tau) - V_{Se}(S_e, S_g, L, \tau) \\ \frac{\partial G}{\partial z_g}(0, z_g) &= V_{S_g}(S_e, S_g + z_g, L, \tau) - V_{Sg}(S_e, S_g, L, \tau) \\ \frac{\partial^2 G}{\partial z_e \partial z_g}(z_e, z_g) &= V_{S_e S_g}(S_e + z_e, S_g + z_g, L, \tau) \end{aligned} \quad (50)$$

So, after the substitution of eqs. (49) and (50) in equation (41) our HJB PIDE becomes

$$\begin{aligned} V_\tau = \frac{1}{2}\sigma_e^2 V_{S_e S_e} + \frac{1}{2}\sigma_g^2 V_{S_g S_g} + \rho\sigma_e\sigma_g V_{S_e S_g} + \mu_e(S^e, T-\tau)V_{S_e} + \mu_g(S^g, T-\tau)V_{S_g} - rV + \\ \int_{\mathbb{R}_+} (V_{S_e}(S_e + z_e, S_g, L, \tau) - V_{S_e}(S_e, S_g, L, \tau))\nu_e((dz_e) \\ + \int_{\mathbb{R}_+} (V_{S_g}(S_e, S_g + z_g, L, \tau) - V_{S_g}(S_e, S_g, L, \tau))\nu_g(dz_g) \\ + \int_{\mathbb{R}^2_+} V_{S_e S_g}(S_e + z_e, S_g + z_g, L, \tau)F(U_1(z_e), U_2(z_g))dz_e dz_g \\ \max_c [H(L)S_e - S_g c + \eta(L, c)(\bar{L}(c) - L)V_L] \end{aligned} \quad (51)$$

We assumed in Section 2 that $L_e(t)$ and $L_g(t)$ were compound Poisson processes with intensities λ_e and λ_g and jump size distributions D_e and D_g. Then the tail integrals of $L_e(t)$ and $L_g(t)$ are

$$U_1(x) = \lambda_e(1 - D_e(x)), \quad (52)$$

$$U_2(x) = \lambda_g(1 - D_g(x)), \quad (53)$$

respectively. If we substitute U_1 and U_2 in the formula (46) for the skewed Clayton- Lévy copula we get

$$F(U_1(z_e), U_2(z_g)) = ((\alpha U_2^{-\beta} + 1)U_1^{-\theta} + U_2^{-\theta})^{-1/\theta} = \left(\left(\frac{\alpha}{\lambda_g^{\beta}(1 - D_g(z_g))^{\beta}} + 1\right)\frac{1}{\lambda_e^{\theta}(1 - D_e(z_e))^{\theta}} + \frac{1}{\lambda_g^{\theta}(1 - D_g(z_g))^{\theta}}\right)^{-\frac{1}{\theta}}, \quad (54)$$

which is a two-dimensional function depending on z_e and z_g. We will make use of this formula later in Section 6 in our numerical approximations.

5 Boundary conditions

The terminal condition for our power plant valuation is assumed to be

$$V(S_e, S_g, L, \tau = 0) = 0. \quad (55)$$

where $\tau = T - t$. Based on Thompson et al. (2004), Safarov & Atkinson (2016) we choose the following limits as the boundary conditions:

$$\begin{aligned} S_e \to 0 \quad \text{or} \quad S_e \to \infty \Longrightarrow \quad V_{S_eS_e} \to 0 \quad \text{and} \quad V_{S_eS_g} \to 0 \\ S_g \to 0 \quad \text{or} \quad S_g \to \infty \Longrightarrow \quad V_{S_gS_g} \to 0 \quad \text{and} \quad V_{S_eS_g} \to 0 \end{aligned} \quad (56)$$

The domain of the HJB equation (51) is $S_e \times S_g \times L = [0, \infty) \times [0, \infty) \times [L_{\min}, L_{\max}]$ But we need bounded domain for numerical calculations. So we need to restrict this unbounded domain to $[0, S_e^{\max},) \times [0, S_g^{\max}) \times [L_{\min}, L_{\max}]$. Hence, for the case $S_e \to 0$ we apply $V_{S_eS_e} \to 0$ and $V_{S_eS_g} \to 0$ to simplify equation (51) to

$$V_\tau = \frac{1}{2}\sigma_g^2 V_{S_gS_g} + \mu_e(0, T - \tau)V_{S_e} + \mu_g(S^g, T - \tau)V_{S_g} - rV + \int_{\mathbb{R}} (V_{S_g}(0, S_g + z_g, L, \tau) - V_{S_g}(0, S_g, L, \tau))\nu_g(dz_g) + \max_c[-S_g c + \eta(L, c)(\bar{L}(c) - L)V_L] \quad (57)$$

For the case $S_e \to S_e^{\max}$ we employ the first line of (56) again to get

$$V_\tau = \frac{1}{2}\sigma_g^2 V_{S_gS_g} + \mu_e(S_e^{\max}, T - \tau)V_{S_e} + \mu_g(S^g, T - \tau)V_{S_g} - rV + \int_{\mathbb{R}} (V_{S_g}(S_e^{\max}, S_g + z_g, L, \tau) - V_{S_g}(S_e^{\max}, S_g, L, \tau))\nu_g(dz_g) + \max_c[H(L)S_e^{\max} - S_g c + \eta(L, c)(\bar{L}(c) - L)V_L] \quad (58)$$

We can obtain the boundary conditions for the limits $S_g \to 0$ and $S_g \to S_g^{\max}$ in a similar way. To conclude our analysis of boundary conditions we need to

construct the equations corresponding to 4 corner points: $(S_e, S_g) \to (0,0)$, $(S_e, S_g) \to (0, S_g^{\max})$, $(S_e, S_g) \to (S_e^{\max}, 0)$ and $(S_e, S_g) \to (S_e^{\max}, S_g^{\max})$. For the first two corners we have

$$V_\tau = \mu_e(0, T-\tau)V_{S_e} + \mu_g(0, T-\tau)V_{S_g} - rV + \max_c[\eta(L,c)(\bar{L}(c) - L)V_L] \quad (59)$$

and

$$V_\tau = \mu_e(0, T-\tau)V_{S_e} + \mu_g(S_g^{\max}, T-\tau)V_{S_g} - rV + \max_c[-S_g^{\max}c + \eta(L,c)(\bar{L}(c) - L)V_L] \quad (60)$$

Similarly, we can derive the equations for the other two corners.

6 Discretisation scheme

L^e and L^g are finite activity Lévy processes where $\nu_e(\mathbb{R}_+) = \lambda_e$ and $\nu_g(\mathbb{R}_+) = \lambda_g$. Therefore, we can rewrite the single integral terms of equation (51) as

$$\int_{\mathbb{R}_+} (V_{S_e}(S_e + z_e, S_g, L, \tau) - V_{S_e}(S_e, S_g, L, \tau))\nu_e(dz_e) = \int_{\mathbb{R}_+} V_{S_e}(S_e + z_e, S_g, L, \tau)\nu_e(dz_e) - \lambda_e V_{S_e}(S_e, S_g, L, \tau) \quad (61)$$

and

$$\int_{\mathbb{R}_+} (V_{S_g}(S_e, S_g + z_g, L, \tau) - V_{S_g}(S_e, S_g, L, \tau))\nu_g(dz_g) = \int_{\mathbb{R}_+} V_{S_g}(S_e, S_g + z_g, L, \tau)\nu_g(dz_g) - \lambda_g V_{S_g}(S_e, S_g, L, \tau) \quad (62)$$

If we substitute eqs. (61) and (62) in equation (51) the coefficients of partial derivatives V_{S_e} and V_{S_g} modify to

$$\bar{\mu}_e(S^e, t) = \bar{\Lambda}_e(t) - \alpha_e S^e(t) - \lambda_e \quad (63)$$

$$\bar{\mu}_g(S^g, t) = \bar{\Lambda}_g(t) - \alpha_g S^g(t) - \lambda_g \quad (64)$$

and the HJB equation (51) can be written as

$$V_\tau = \mathcal{D}V + \mathcal{H}_e V + \mathcal{H}_g V + \mathcal{H}_{eg} V + \max_c[H(L)S_e - S_g c + \eta(L,c)(\bar{L}(c) - L)V_L] \quad (65)$$

where

$$\begin{aligned}\mathcal{D}V =&\frac{1}{2}\sigma_e^2 V_{S_eS_e} + \frac{1}{2}\sigma_g^2 V_{S_gS_g} + \rho\sigma_e\sigma_g V_{S_eS_g} + \\ &\mu_e(S^e, T-\tau)V_{S_e} + \mu_g(S^g, T-\tau)V_{S_g} - rV \end{aligned} \tag{66}$$

$$\mathcal{H}_eV = \int_{\mathbb{R}_+} V_{S_e}(S_e + z_e, S_g, L, \tau)\nu_e((dz_e), \tag{67}$$

$$\mathcal{H}_gV = \int_{\mathbb{R}_+} V_{S_g}(S_e, S_g + z_g, L, \tau)\nu_g(dz_g) \tag{68}$$

and

$$\mathcal{H}_{eg}V = \int_{\mathbb{R}_+^2} V_{S_eS_g}(S_e + z_e, S_g + z_g, L, \tau)F(U_1(z_e), U_2(z_g))dz_e dz_g \tag{69}$$

Note that we dropped the bar signs from our coefficients $\bar{\mu}_e$ and $\bar{\mu}$ for simplicity. We will apply the explicit finite difference scheme proposed in Cont & Voltchkova (2005*a*,*b*) to deal with the diffusion $\mathcal{D}V$ and single integral terms $\mathcal{H}_eV$ and $\mathcal{H}_gV$. The discretisation of $\mathcal{H}_{eg}V$ and optimisation terms requires further analysis.

First of all, we need to discretise the domain of the HJB equation by the following grid:

$$\begin{aligned}&\tau_n = n\Delta\tau, \quad n = 0, \dots, M, \quad \Delta\tau = \frac{T}{M}, \\ &S_i^e = i\Delta S^e, \quad i = 0, \dots, N_e, \quad \Delta S^e = \frac{S^e_{\max}}{N_e}, \\ &S_j^g = j\Delta S^g, \quad j = 0, \dots, N_g, \quad \Delta S^g = \frac{S^g_{\max}}{N_g}, \\ &L_u = L_{\min} + u\Delta L, \quad u = 0, \dots, L, \quad \Delta L = \frac{L_{max} - L_{\min}}{N_L}. \end{aligned} \tag{70}$$

So, $V(S_i^e, S_j^g, L_u, \tau_n) = V(i\Delta S^e, j\Delta S^g, u\Delta L, n\Delta\tau)$ is the exact solution of equation (51) at the node $(S_i^e, S_j^g, L_u, \tau_n)$, while $V_{i,j,u}^n$ stands for the approximate solution at the same node.

For the diffusion/PDE part we follow the steps discussed in Safarov & Atkinson (2016) use the explicit method discussed in Safarov & Atkinson (2016) and apply similar corrector term to get rid off the monotonicity issue. In other words,

$$\begin{aligned}&\mathcal{D}V_{i,j,u}^n = \frac{\sigma_e^2}{2\Delta S_e^2}(V_{i+1,j,u}^n - 2V_{i,j,u}^n + V_{i-1,j,u}^n) + \frac{\sigma_g^2}{2\Delta S_g^2}(V_{i,j+1,u}^n - 2V_{i,j,u}^n + V_{i,j-1,u}^n) + \\ &\frac{\rho\sigma_e\sigma_g}{4\Delta S_e\Delta S_g}(V_{i+1,j+1,u}^n + V_{i-1,j-1,u}^n - V_{i,j+1,u}^n - V_{i,j-1,u}^n - V_{i+1,j,u}^n - V_{i-1,j,u}^n + 2V_{i,j,u}^n) + \\ &\frac{\mu_e(S_i^e, T-\tau_n)}{\Delta S_e}(V_{i+1,j,u}^n - V_{i,j,u}^n) + \frac{\mu_g(S_j^g, T-\tau_n)}{\Delta S_g}(V_{i,j+1,u}^n - V_{i,j,u}^n) - rV_{i,j,u}^n \end{aligned} \tag{71}$$

assuming that $\mu_e \geq 0$ and $\mu_g \geq 0$. We will use the downwind scheme for the cases $\mu_e \leq 0$ and $\mu_g \leq 0$.

For the integral terms $\mathcal{H}_e V$ and $\mathcal{H}_g V$ we first need to restrict the unbounded integration domains by setting finite upper bounds B_e and B_e to truncate the larger jumps. We employ the trapezoidal quadrature method in order to get the numerical approximations for these integrals and take $\Delta z_e = \Delta S_e$ and $\Delta z_g = \Delta S_g$. We also choose positive integers K_e and K_g such that $[0, B_e] \subset [0, (K_e + \frac{1}{2})\Delta z_e]$ and $[0, B_g] \subset [0, (K_g + \frac{1}{2})\Delta z_g]$, respectively. By using the central difference discretisation for the partial derivatives V_{S_e} and V_{S_g} we get

$$\begin{aligned}
\mathcal{H}_e V^n_{i,j,u} =& \int_0^{B_e} V_{S_e}(S^e_i + z_e, S^g_j, L_u, \tau_n)\nu_e((dz_e) \\
=& \frac{1}{2\Delta S_e}\int_0^{B_e} (V(S^e_{i+1} + z_e, S^g_j, L_u, \tau_n) - V(S^e_{i-1} + z_e, S^g_j, L_u, \tau_n))\nu_e((dz_e) \\
\approx& \frac{1}{2\Delta S^e}(\sum_{k=0}^{K_e} \nu^e_k V^n_{i+k+1,j,u} - \sum_{k=0}^{K_e} \nu^e_k V^n_{i+k-1,j,u}) \qquad (72)
\end{aligned}$$

and

$$\begin{aligned}
\mathcal{H}_g V^n_{i,j,u} =& \int_0^{B_g} V_{S_g}(S^e_i, S^g_j + z_g, L_u, \tau_n)\nu_g((dz_g) \\
=& \frac{1}{2\Delta S_g}\int_0^{B_g} (V(S^e_i, S^g_{j+1} + z_g, L_u, \tau_n) - V(S^e_i, S^g_{j-1} + z_g, L_u, \tau_n))\nu_g((dz_e) \\
\approx& \frac{1}{2\Delta S_g}(\sum_{k=0}^{K_g} \nu^g_k V^n_{i,j+k+1,u} - \sum_{k=0}^{K_g} \nu^g_k V^n_{i,j+k-1,u}) \qquad (73)
\end{aligned}$$

where

$$\nu^e_k = \int_{(k-\frac{1}{2})\Delta S_e}^{(k+\frac{1}{2})\Delta S_e} \nu_e(dz_e) \quad \text{and} \quad \nu^g_k = \int_{(k-\frac{1}{2})\Delta S_g}^{(k+\frac{1}{2})\Delta S_g} \nu_g(dz_g) \qquad (74)$$

We can now go through the numerical calculation of the double integral

$$\mathcal{H}_{eg} V = \int_0^{B_e}\int_0^{B_g} V_{S_e S_g}(S_e + z_e, S_g + z_g, L, \tau) F(U_1(z_e), U_2(z_g)) dz_e dz_g \qquad (75)$$

First of all, denote $\bar{F}(z_e, z_g) = F(U_1(z_e), U_2(z_g))$ for clarity purposes. Then apply the central difference formula to approximate the cross-derivative $V_{S_e S_g}$ at the node $(S^e_i + z_e, S^g_j + z_g, L_u, \tau_n)$:

$$\begin{aligned}
V_{S_e S_g}(S^e_i + z_e, S^g_j + z_g, L_u, \tau_n) \approx \frac{1}{4\Delta S_e \Delta S_g}(&V(S^e_{i+1} + z_e, S^g_{j+1} + z_g, L_u, \tau_n) - \\
V(S^e_{i+1} + z_e, S^g_{j-1} + z_g, L_u, \tau_n) &- V(S^e_{i-1} + z_e, S^g_{j+1} + z_g, L_u, \tau_n) \\
&+ V(S^e_{i-1} + z_e, S^g_{j-1} + z_g, L_u, \tau_n)) \qquad (76)
\end{aligned}$$

By taking the double integral of both sides above we get

$$\mathcal{H}_{eg}V \approx \frac{1}{4\Delta S_e \Delta S_g}\int_0^{B_e}\int_0^{B_g}(V(S^e_{i+1}+z_e, S^g_{j+1}+z_g, L_u, \tau_n) - V(S^e_{i+1}+z_e, S^g_{j-1}+z_g, L_u, \tau_n) - V(S^e_{i-1}+z_e, S^g_{j+1}+z_g, L_u, \tau_n) + V(S^e_{i-1}+z_e, S^g_{j-1}+z_g, L_u, \tau_n))\bar{F}(z_e, z_g)dz_e dz_g \quad (77)$$

Thus, we need to integrate 4 terms over $[0, B) \times [0, B)$ in equation (77) in order to evaluate $\mathcal{H}_{eg}V$. For this purpose we will make use of two-dimensional trapezoidal rule explained below (see Davis & Rabinowitz 2007).

Let $f(x, y)$ be given over the rectangle $\{(x, y) : 0 \le x \le a, 0 \le y \le b\}$. Assume that the intervals $[0, a]$ and $[0, b]$ are equally subdivided into K_1 and K_2 subintervals with widths $h_1 = \frac{a}{K_1}$ and $h_2 = \frac{b}{K_2}$, respectively. The sample points x_i and y_j are defined as $x_i = ih_1$ and $y_j = jh_2$ where $i = 0, \dots K_1$ and $j = 0, \dots K_2$. Then the two-dimensional trapezoidal rule can be formulated as follows

$$\int_0^a \int_0^b f(x, y)dxdy \approx \sum_{i=0}^{K_1}\sum_{j=0}^{K_2}\omega_{ij} f(x_i, y_j)h_1 h_2 \quad (78)$$

where

$$\omega_{ij} = \begin{cases} 1 & \text{for} \quad 0 < i < K_1 \quad \text{and} \quad 0 < j < K_2 & \text{interior} \\ \frac{1}{2} & \text{for} \quad (0, j) \quad \text{or} \quad (i, 0) & \text{exterior} \\ \frac{1}{4} & \text{fpr} \quad (i, j) \in \{(0, 0), (N_B, N_B)\} & \text{corners.} \end{cases} \quad (79)$$

We apply this integration rule to approximate the four terms on the right hand side (RHS) of equation (77). Let's first consider the first term

$$f(z_e, z_g) = V(S^e_{i+1}+z_e, S^g_{j+1}+z_g, L_u, \tau_n)\bar{F}(z_e, z_g) \quad (80)$$

This is a two-dimensional function depending on z_e and z_g. So, we can apply the 2d trapezoidal rule to get

$$\int_0^{B_1}\int_0^{B_2} V(S^e_{i+1}+z_e, S^g_{j+1}+z_g, L_u, \tau_n)\bar{F}(z_e, z_g)dz_e dz_g \approx \sum_{k_1=0}^{K_1}\sum_{k_2=0}^{K_2} V(S^e_{i+k_1+1}, S^g_{j+k_2+1}, L_u, \tau_n)\bar{F}(S^e_{k_1}, S^g_{k_2})h_1 h_2 \omega_{k_1 k_2} \quad (81)$$

We can similarly calculate the other three terms.

Hence, after denoting the approximate value of $c(S^e_i, S^g_j, L_u, \tau_n)$ by $\Omega^n_{i,j,u}$ our explicit scheme becomes

$$\frac{V^{n+1}_{i,j,u} - V^n_{i,j,u}}{\Delta\tau} = DV^n_{i,j,u} + H_e V^n_{i,j,u} + H_g V^n_{i,j,u} + H_{eg}V^n_{i,j,u} + \max_{\Omega^n_{i,j,u} \in C(I)}\left\{H(L_u)S^e_i - S^g_j\Omega^n_{i,j,u} + \eta(L_u, \Omega^n_{i,j,u})(\bar{L}(\Omega^n_{i,j,u}) - L_u)\frac{V^n_{i,j,u+1} - V^n_{i,j,u}}{\Delta L}\right\} \quad (82)$$

where D, H_e, H_g and H_{eg} are discretisation operators corresponding to $\mathcal{D}, \mathcal{H}_e, \mathcal{H}_g$ and $\mathcal{H}_{eg}$, respectively. Note that when $\eta(L_u, \Omega^n_{i,j,u})(\bar{L}(\Omega^n_{i,j,u}) - L_u) < 0$ we will discretise V_L by $(V^n_{i,j,u} - V^n_{i,j,u-1})/\Delta L$.

We know from the initial condition that $V^0_{i,j,u} = 0$. So, starting from time $\tau_0 = 0$ we first solve the maximization problem

$$\hat{\Omega}^n_{i,j} = \underset{\Omega^n_{i,j,u} \in C(I)}{\arg\max} \left\{ H(L_u) S^e_i - S^g_j \Omega^n_{i,j,u} + \eta(L_u, \Omega^n_{i,j,u})(\bar{L}(\Omega^n_{i,j,u}) - L_u) \frac{V^n_{i,j,u+1} - V^n_{i,j,u}}{\Delta L} \right\}, \tag{83}$$

then substitute this optimal strategy $\hat{\Omega}^n_{i,j}$ in (82) to get

$$V^{n+1}_{i,j,u} = V^n_{i,j,u} + \Delta\tau(DV^n_{i,j,u} + H_e V^n_{i,j,u} + H_g V^n_{i,j,u} + H_{eg} V^n_{i,j,u}) +$$
$$\Delta\tau \left\{ H(L_u) S^e_i - S^g_j \hat{\Omega}^n_{i,j,u} + \eta(L_u, \hat{\Omega}^n_{i,j,u})(\bar{L}\hat{\Omega}^n_{i,j,u}) - L_u) \frac{V^n_{i,j,u+1} - V^n_{i,j,u}}{\Delta L} \right\} \tag{84}$$

where $n = 0, 1, ..., M-1$.

7 Hypothetical gas-fired power plant example

As we mentioned earlier, we want to model the power output as a function of heat L. We specifically refer to Thompson et al. (2004) in assuming

$$H(L) = \begin{cases} 0 & \text{for} \quad L < 300 \\ \frac{5}{6}L - 100 & \text{for} \quad 300 \leq L \leq 600 \end{cases} \tag{85}$$

Hence, the minimum and maximum operating temperatures for electricity generation are 300°C and 600°C, respectively which correspond to 150 MW and 400 MW output levels. As we are dealing with a dynamic model, we also need the equilibrium temperature for the boiler that depends on the amount of burned gas c:

$$\bar{L}(c) = b_0 - b_1(c - b_2)^2, \tag{86}$$

where $(b_0, b_1, b_2) = (650, 0.00003571, 4200)$. By assuming $\eta(L, c) = \eta = 0.1$ in equation (28) we get the following dynamics for the temperature

$$\frac{dL}{dt} = 0.1(\bar{L}(c) - L), \tag{87}$$

where $0 \leq c \leq 3017$. We then impose a ramp rate restriction

$$\left| \frac{dL}{dt} \right| \leq 15. \tag{88}$$

proposed by Thompson et al. (2004). If we combine this restriction with (87), we can update the lower and upper boundaries for the control variable c in the following way

$$\bar{c}_{\min}(L) \leq c \leq \bar{c}_{\max}(L), \qquad 20 \leq L \leq 600 \tag{89}$$

where

$$\bar{c}_{\min}(L) = \max\left(0, 4200 - 100\sqrt{\frac{800-L}{0.3571}}\right), \tag{90}$$

$$\bar{c}_{\max}(L) = \min\left(3017, 4200 - 100\sqrt{\frac{500-L}{0.3571}}\right) \tag{91}$$

Note the discontinuity of $H(L)$ at $L = 300$ causes some oscillation problems related to the discretisation of the partial derivative V_L. with the smothness of solutions. We will follow Thompson et al. (2004) in making use of minmod slope limiters to get rid off this smoothness issue. The detailed explanation regarding slope or flux limiters is provided by LeVeque (1992).

7.1 Slope limiter

The following calculations do not affect the diffusion and integration parts of equation (51). Therefore, we can omit them in order to simplify our PIDE to

$$V_\tau = H(L)S_e - S_g c^* + \eta(L, c^*)(\bar{L}(c^*) - L)V_L] \tag{92}$$

If we denote $a(L) = \eta(L, c^*)(\bar{L}(c^*) - L)$ in equation (92) then we can see that

$$V_\tau = H(L)S_e - S_g c^* + a(L)V_L] \tag{93}$$

is an advection equation with variable speed $a(L)$. According to equation (84), we find c^* before applying explicit scheme to discretise (93). Therefore, we can extend the MUSCL scheme (Monotonic Upwind-Centered Scheme for Conservation Laws) for advection equations with constant speed to cover equation (93) as well. So,

$$V_u^{n+1} = V_u^n + \Delta\tau(H(L_u)S_i^e - S_j^g\hat{\Omega}_u^n) - \zeta(V_{u_1}^n - V_{u_1-1}^n) - \frac{1}{2}\zeta(\text{sign}(\zeta) - \zeta)\Delta L(\sigma_{u_1} - \sigma_{i_1-1}), \tag{94}$$

where $\zeta = \frac{\Delta\tau a(L_u)}{\Delta L}$ and

$$u_1 = \begin{cases} u & \text{if} \quad \zeta > 0 \\ u+1 & \text{if} \quad \zeta \leq 0. \end{cases} \tag{95}$$

σ_u^n is some slope that needs to be defined in order to reduce the numerical oscillations. The oscillations in a solution are measured by the total variation (TV) of V:

$$TV(V) = \sum_{u=1}^{N} |V_u - V_{u-1}| \tag{96}$$

The increase of TV leads to the development of oscillations in a solution. Therefore, a numerical method is total variation diminishing (TVD) if

$$TV(V^{n+1}) \leq TV(V^n) \tag{97}$$

We need to limit the slope σ_u^n of the MUSCL scheme to make it TVD. One of such ways is the minmod slope limiter:

$$\sigma_u^n = \text{minmod}\left(\frac{V_u^n - V_{u-1}^n}{\Delta L}, \frac{V_{u+1}^n - V_u^n}{\Delta L}\right) \tag{98}$$

where

$$\begin{aligned}\text{minmod}(a,b) &= \begin{cases} a & \text{if} \quad |a| < |b| \quad \text{and} \quad ab > 0 \\ b & \text{if} \quad |a| > |b| \quad \text{and} \quad ab > 0 \\ 0 & \text{if} \quad ab \leq 0 \end{cases} \\ &= \frac{1}{2}(\text{sign}(a) + \text{sign}(b))\min(|a|, |b|). \end{aligned} \tag{99}$$

Thus, after improving the numerical algorithm (84) via the minmod slope limiter technique, we can get benefit from the accuracy of second order differencing scheme while avoiding numerical oscillations.

7.2 Numerical results

We first consider the framework similar to the one presented in Thompson et al. (2004). More precisely, we assume that the natural gas spot price is constant $S_g = 3.5 MMBtu$ and the input parameters are

$$(\alpha_e, \sigma_e, \lambda_e, T, r) = (.1, .12, .1, 200\ hours, .05). \tag{100}$$

Moreover, power spot price jump sizes are normally distributed, $\mathcal{N}(700, 100^2)$. The deterministic seasonality function Λ_e is given as

$$\Lambda_e(t) = 15\sin((2\pi t - 15.4\pi)/24) + 27, \tag{101}$$

The optimal operating strategy surface for the gas-fired power plant is presented in Figure 2. For boiler temperatures below 300°C the optimal strategy is to burn maximum amount of fuel within physical limitations in order to keep the plant on line. For low electricity spot prices gas consumption decreases when the temperature is above the minimum operation level to minimise the cost. But for higher power prices the optimal control of gas consumption increases nonlinearly with respect to spot prices and temperature. We can see from Figure 2 that in the case of low electricity spot prices the power plant burns more fuel for very high temperatures. This strategy is explained by the ramp rate restriction. In other words, we can't shut down the plant immediately when the boiler is close to its maximum temperature limit. It will take some time for the unit to cool and we have to burn the required amount of gas during that time period.

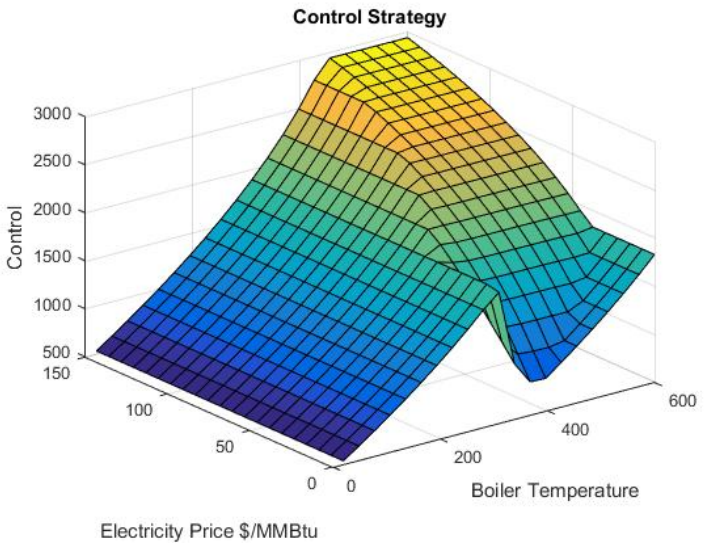


Figure 2: The optimal operating strategy surface for the gas-fired power plant for fixed gas price $S_g = 3.5$. When the boiler temperature is below 300°C the optimal strategy is to consume maximum amount of gas within physical limitations to keep the plant on line. For low electricity spot prices gas consumption decreases when the temperature is above the minimum operation level to minimise the cost and increases for very high temperatures due to the ramp rate constraint. But for higher power prices the optimal control of gas consumption increases nonlinearly with respect to spot prices and temperature.

The Figure 3 shows the value or expected cash flow surface of power generating facility. We can see that the value surface does not depend on electricity spot prices when the boiler temperature is below the operating level. The plant is not reacting to spot price changes because there is no guarantee that by the time we increase the temperature to 300°C spot prices will remain the same. Beyond 300°C the plant starts to generate electricity which explains the non-smooth behaviour of the value surface at $L = 300$. Beyond this line both higher power prices and boiler temperatures contribute to larger values of the power generator. Thus, our optimal control and value surfaces look similar to the figures given by Thompson et al. (2004). Unfortunately, we can't conduct more accurate comparison due to some missing parameter specifications in the original paper.

We can now investigate the numerical calculations for the underlying spot price models (12) and (15). The parameters for our single regime model are given in Table 1. We assume that the risk-free interest rate is the same, $r = 0.05$. As the jump size distributions D_e and D_g we take inverse Gaussian distributions $IG(\mu, \lambda)$ where $\mu > 0$ and $\lambda > 0$ are mean and shape parameters, respectively. We can use the parameter values $(.60, .56)$ and $(.54, .32)$ for the corresponding

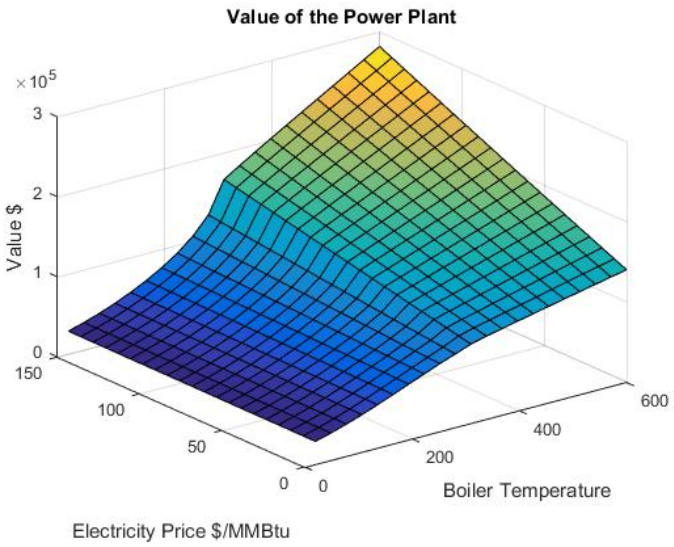


Figure 3: The value surface of power generating facility for fixed gas price $S_g = 3.5$. The surface does not depend on power prices when the boiler temperature is below the operating level. Beyond 300°C the plant starts to generate electricity which explains the non-smooth behaviour of the value surface at $L = 300$. Both higher power prices and boiler temperatures result in larger values of the power generator.

distributions of power and gas price jumps.

Meanwhile, the deterministic seasonality terms Λ_e and Λ_g will be defined as follows

$$\Lambda_e(t) = 15\sin((2\pi t - 15.4\pi)/24) + 27, \tag{102}$$

$$\Lambda_g(t) = 0.6\cos(2\pi(t - 18\pi)/24) + 2.7 \tag{103}$$

Figure 4 compares optimal operating surfaces with respect to power prices and boiler temperature for various gas spot prices. When $S_g \to 0$, the generation costs are so small that the plant burns gas as much as possible at all levels of power prices and temperatures (Figure 4a). Figure 4b depicts the case when

Parameter	Value	Parameter	Value
α_e	.1	λ_e	.1
α_g	.23	λ_g	.4
σ_e	.11	T	200 hours
σ_g	.09	ρ	.15

Table 1: Input parameters for the single regime power plant model.

S_g = 10\$/MMBtu. We can see that the surface looks more like in 2. For higher levels of natural gas spot prices the region of intensive fuel consumption diminishes (Figure 4c and 4d).

Value surfaces with respect to power spot price and boiler temperature for different gas prices are depicted in Figure 5. The shapes of these surfaces are almost the same. As gas prices increase, the surfaces shift downwards. But when S_g is too high, the power plant value becomes dependent on power spot prices even for low temperature levels (Figure 5c).

In Figure 6 we can observe optimal control and corresponding value surfaces with respect to gas spot price and boiler temperature for different electricity prices. Figures (a)-(c) imply that the higher is S_e, the larger is the maximum consumption region. For very low values of electricity the plant minimises its fuel cost even before reaching 300°C. But when the power prices are too high the plant can keep burning gas at full capacity beyond 300°C as well. Running the plant in the presence of extremely expensive fuel prices when the boiler temperature is too high becomes unbearable. Therefore, the optimal strategy is to reduce gas consumption to minimum.

We can see from Figures 6(d)-(f) that value surfaces shift upwards when S_e increases. Meanwhile, the value surface doesn't exhibits a sharpe change in $L = 300$°C when power prices are too low. In this case the surface becomes dependent on gas prices for boiler temperatures below the operating level. This dependence vanishes away for higher values of S_e.

The operating strategies with respect to electricity and gas spot prices for different boiler temperatures are depicted in Figure 7. For very low boiler temperatures the control strategy surface is flat. In other words, it doesn't change depending on underlying spot prices. Starting from the case $L = 300$°C we notice a small region of dependence on power and gas spot prices. For higher temperature levels we can see that dependence more clearly (Figures 7c and 7d).

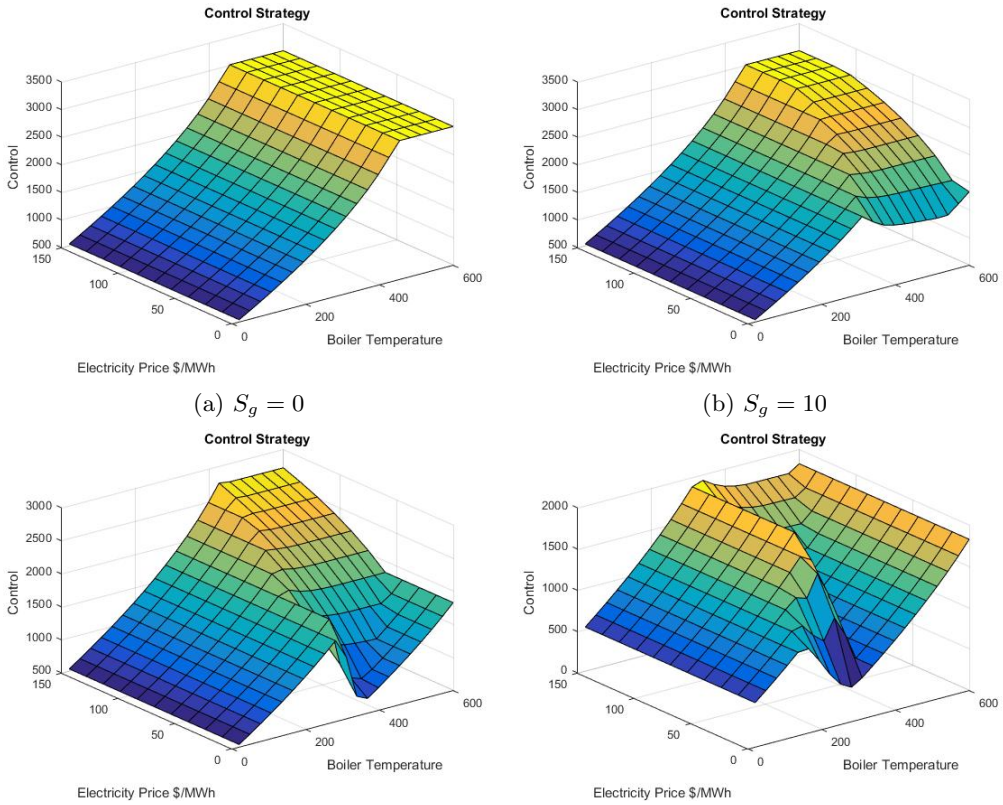
We can differentiate 3 different regions here: $c_{\min}$ (dark blue), $c_{\max}$ (yellow), and $c_{min} \leq c \leq c_{max}$ (in between).

Figure 8 describes the power generator value surface with respect to electricity and gas spot prices when $L = 320$°C. The value surface exhibits increasing and decreasing dependence on power and natural gas spot prices, respectively. The overall shape of the surface is the same for other temperature levels as well.

8 Regime switching

Let's assume the economy has two phases/regimes (0 and 1) and the switch has some finite probabilities: $\lambda^{0\to1}dt$ and $\lambda^{1\to0}dt$. We will model this regime switching by the following two state continuous-time Markov chain $m(t)$ presented by Chen & Forsyth (2010):

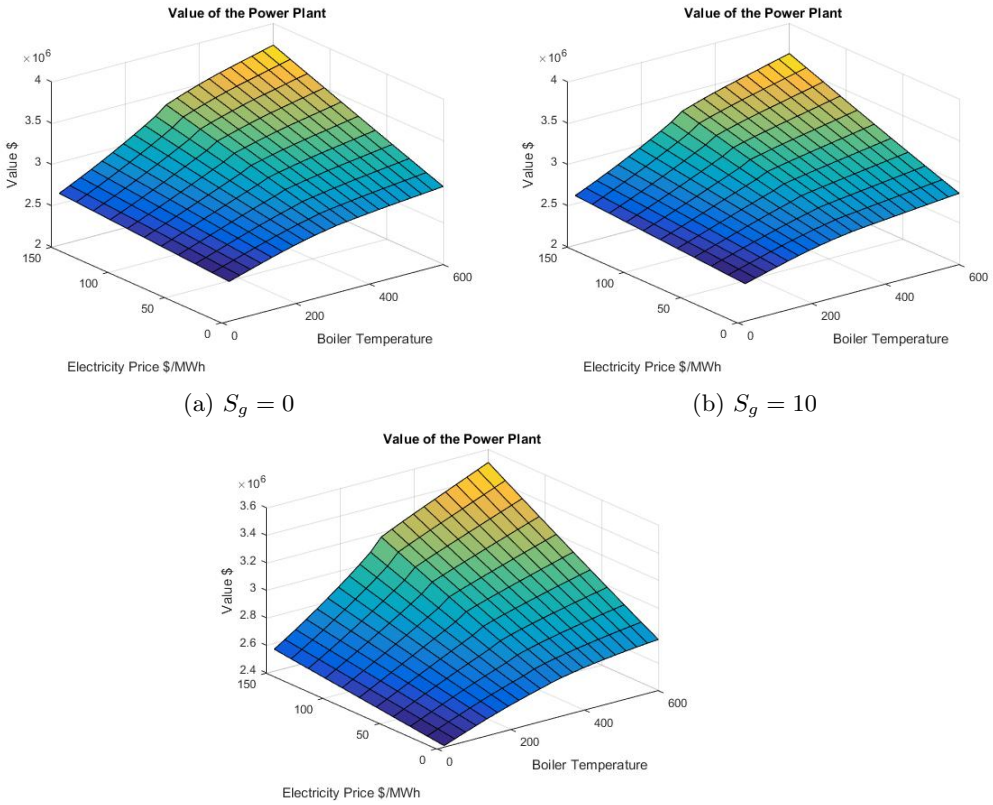
$$dm(t) = (1 - m(t-))dN^{0\to1} - m(t-)dN^{1\to0} \tag{104}$$



(a) $S_g = 0$ (b) $S_g = 10$

(c) $S_g = 14$ (d) $S_g = 20$

Figure 4: Optimal operating strategy for the single regime model with respect to electricity spot price and boiler temperature for different gas prices. When $S_g \to 0$, the power generation costs are negligible. Therefore, the plant burns gas as much as possible at all levels of electricity prices and temperatures (a). The surface looks more like in Figure 2 when $S_g = 10\$/\text{MMBtu}$ (b). The region of intensive gas consumption diminishes for higher levels of natural gas spot prices ((c) and (d)).

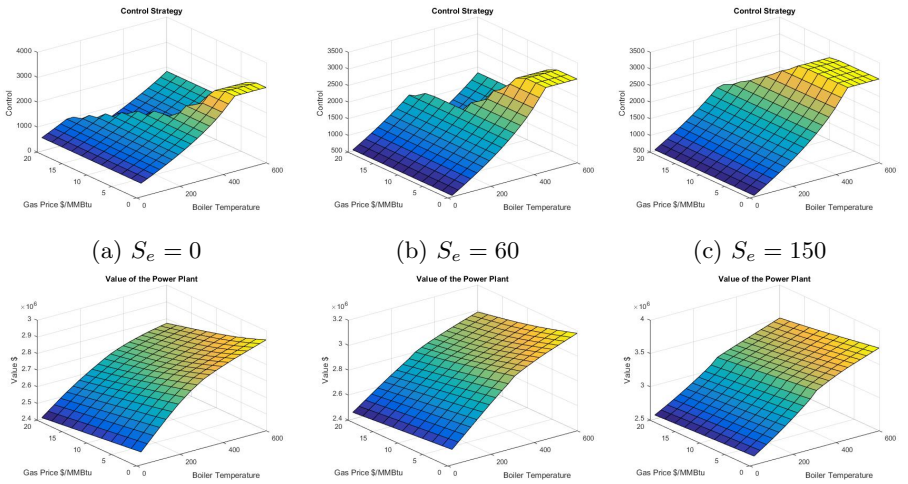


(a) $S_g = 0$

(b) $S_g = 10$

(c) $S_g = 20$

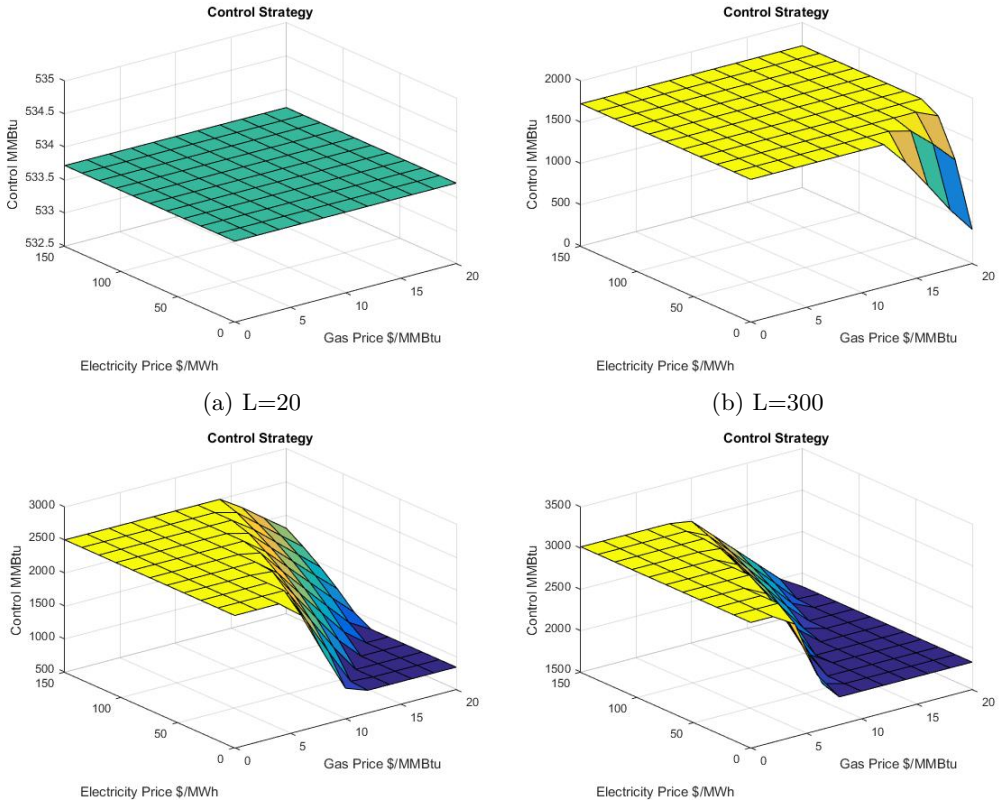
Figure 5: Value surface of the power plant for the single regime model with respect to electricity spot price and boiler temperature for different gas prices. The shapes of these surfaces are very similar. As gas prices increase, the surfaces shift downwards ((a) and (b)). But when S_g is too high, the power plant value becomes dependent on power spot prices even for low temperature levels (c).



(a) $S_e = 0$ (b) $S_e = 60$ (c) $S_e = 150$

(d) $S_e = 0$ (e) $S_e = 60$ (f) $S_e = 150$

Figure 6: Operating strategy (a)-(c) and value surfaces (d)-(f) of the power generating facility for a single regime model with respect to gas spot price and boiler temperature for different electricity prices. (a)-(c) imply that the higher is S_e, the larger is the maximum consumption region. The plant minimises its fuel cost even before reaching 300°C for very low values of electricity. When the power prices are too high the plant can keep burning gas at full capacity beyond 300°C as well. In the presence of extremely expensive fuel prices running the plant becomes unbearable if the boiler temperature is too high as well. Thus, the optimal strategy is to reduce gas consumption to minimum. (d)-(f) show that value surfaces shift upwards when S_e increases. Meanwhile, the value surface doesn't exhibits a sharpe change in $L = 300$°C for very low power prices. The surface becomes dependent on gas prices for boiler temperatures below the operating level. This dependence doesn't exist for higher values of S_e.



(a) L=20 (b) L=300

(c) L=420 (d) L=600

Figure 7: Operating strategy for a single regime model with respect to electricity and gas spot prices for different boiler temperatures. For very low boiler temperatures the control strategy surface doesn't change depending on underlying spot prices (a). Starting from the case $L = 300°\text{C}$ a small region of dependence on power and gas spot prices can be noticed ((b) and (c)). The dependence is more clearly visible for higher temperature levels ((c) and (d)).

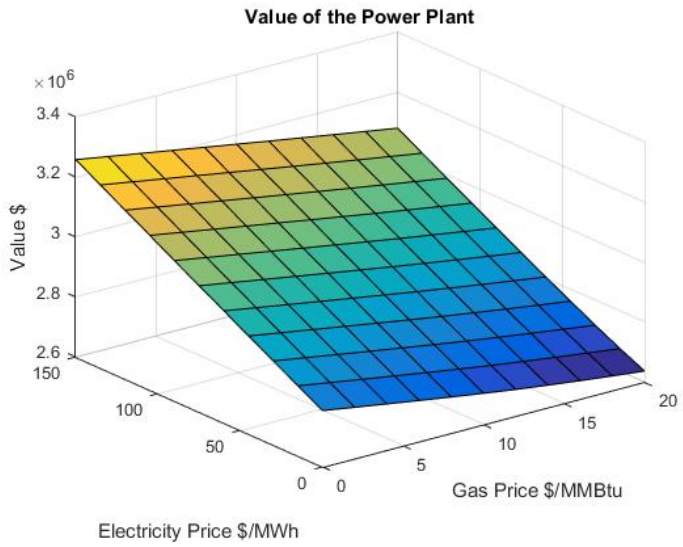


Figure 8: Value surface of the power generator value surface with respect to electricity and gas spot prices when $L = 320°\text{C}$. The value surface exhibits increasing and decreasing dependence on power and natural gas spot prices, respectively.

where $t-$ is the time infinitesimally before t, $N^{0\to1}$ and $N^{1\to0}$ are independent Poisson processes with intensities $\lambda^{0\to1}$ and $\lambda^{1\to0}$,respectively. So, within a regime $l = m(t-)$ the underlying electricity and gas spot prices follow:

$$S^e(t) = \Lambda_e^l(t) + X^e(t) + Y^e(t), \tag{105}$$

where

$$dX^e(t) = -\alpha_e^l X^e(t)dt + \sigma_e^l dB^e(t), \tag{106}$$
$$dY^e(t) = -\alpha_e^l Y^e(t)dt + dL_e^l(t), \tag{107}$$

and

$$S^g(t) = \Lambda_g^l(t) + X^g(t) + Y^g(t), \tag{108}$$

where

$$dX^g(t) = -\alpha_g^l X^g(t)dt + \sigma_g^l dB^g(t), \tag{109}$$
$$dY^g(t) = -\alpha_g^l Y^g(t)dt + dL_g^l(t), \tag{110}$$

where L_e^l and L_g^L are Lévy processes with intensity measures ν_e^l and ν_g^l, respectively. In our compound Poisson case we have

$$\nu_e^l(dz_e) = \lambda_e^l D_e^l(dz_e) \quad \text{and} \quad \nu_g^l(dz_g) = \lambda_g^l D_g^l(dz_g)$$

Parameter	Value	Parameter	Value
α_e	.6	λ_e	.2
α_g	1	λ_g	.6
σ_e	.2	T	200 hours
σ_g	.3	ρ	.15

Table 2: Input parameters for the regime 1 of regime-switching model.

We can rewrite our power plant optimisation objective (29) for each regime l as follows

$$V^l(S_e, S_g, L, t) = \max_{c^l(S_e,S_g,L,t)} \mathbb{E}[\int_t^T e^{-r(\tau-t)}(H(L)S_e - S_g c)d\tau | m(t) = l], \quad (111)$$

subject to

$$c_{min}(L) \leq c^l \leq c_{max}(L). \quad (112)$$

The application of previously used techniques, such as Bellman's Principle of Optimality and Itô's Lemma will give us the following coupled HJB equations

$$\begin{aligned} V^l_\tau = \frac{1}{2}(\sigma^l_e)^2 V^l_{S_eS_e} + \frac{1}{2}(\sigma^l_g)^2 V^l_{S_gS_g} + \rho\sigma^l_e\sigma^l_g V^l_{S_eS_g} + \mu^l_e(S^e, T-\tau)V^l_{S_e} + \\ \mu^l_g(S^g, T-\tau)V^l_{S_g} - rV^l + \lambda^{l\to(1-l)}(V^{(1-l)} - V^l) \\ \int_{\mathbb{R}_+}(V^l_{S_e}(S_e + z_e, S_g, L, \tau) - V^l_{S_e}(S_e, S_g, L, \tau))\nu^l_e((dz_e) \\ + \int_{\mathbb{R}_+}(V^l_{S_g}(S_e, S_g + z_g, L, \tau) - V^l_{S_g}(S_e, S_g, L, \tau))\nu^l_g(dz_g) \\ + \int_{\mathbb{R}^2_+} V^l_{S_eS_g}(S_e + z_e, S_g + z_g, L, \tau)F(U^l_1(z_e), U^l_2(z_g))dz_e dz_g \\ \max_c[H(L)S_e - S_g c + \eta(L,c)(\bar{L}(c) - L)V^l_L] \end{aligned} \quad (113)$$

with the terminal condition

$$V^l(S_e, S_g, L, \tau = 0) = 0. \quad (114)$$

The boundary conditions at each regime will be the same as in Section 5.

8.1 Numerical results

We first need to define our input parameters for the regime switching model. We adopt the parameter values introduced in Section 7.2 for regime 0. Analogously, we make the following assumptions for regime 1 (see Table 2). We assume that the risk-free interest rate is the same, $r = 0.05$. As the jump size distributions D^1_e and D^1_g we again take inverse Gaussian distributions with parameters $(.30, .46)$ and $(.42, .28)$, respectively.

The seasonality terms Λ_e^1 and Λ_g^1 will be assumed to be

$$\Lambda_e^1(t) = 5\sin((2\pi t - 15.4\pi)/24) + 10, \tag{115}$$

$$\Lambda_g^1(t) = 0.3\cos(2\pi(t - 18\pi)/24) + 1.4. \tag{116}$$

Figures 10 and 11 compare operating strategies for the regimes 0 and 1, respectively with respect to power prices and boiler temperature for different gas spot prices. We can see that under both of these regimes the optimal strategy for $S_g \to 0$ is to burn maximum amount of gas all the time. However, for all other non-zero natural gas prices the region of maximum fuel consumption is larger for the regime 0 than for the regime 1. When gas prices are too high the plant no longer consumes fuel when electricity prices are low and $L < 300°\text{C}$. In other words, the plant manager becomes more pessimistic (or risk-averse) under the regime-switching model.

Value surfaces for the regime-switching model with respect to power prices and boiler temperature for the fixed gas price are depicted in Figure 11. The surfaces look similar in their shapes but in regime 1 we have a downside shift which reflects an unfavorable economic situation.

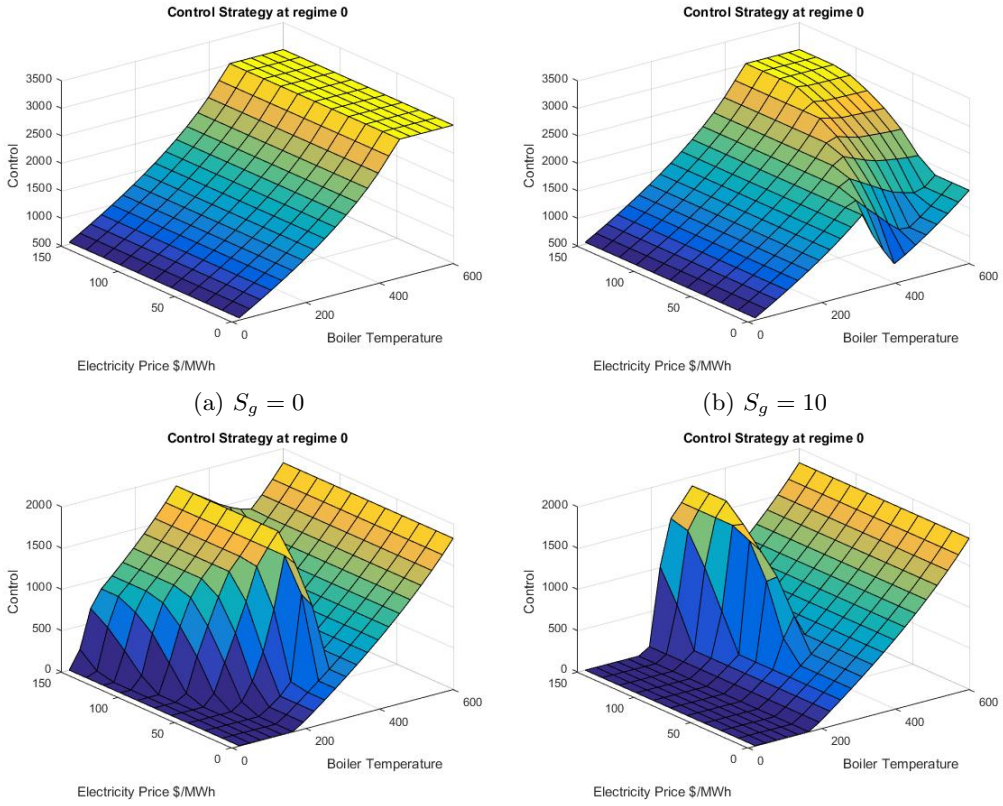
Control strategies for regime-switching model with respect to power and gas spot prices for different boiler temperatures are presented in Figure 12. When the temperature is above the operating level $L = 300°\text{C}$, optimal operation surfaces are more risk-averse in regime 1. As the plant doesn't produce electricity below 300°C, the change in power spot prices does not affect our decision making. Hence, in regime 1 the optimal control surface for $L = 20°\text{C}$ is more optimistic than in regime 0 due to fall in gas spot prices (see Figures 12a and 12d). Moreover, in contrast to Figure 7, the surface isn't flat when the temperature is close to its minimum.

In Figure 13 we can observe operating strategy for regime-switching model with respect to gas spot prices and boiler temperature for different electricity spot prices. In general, these figures show less appealing results than in single regime case (see Figure 6). When the power prices are extremely low or high, the surfaces in regimes 0 and 1 look almost the same. However, for moderate electricity prices we have a larger region of minimal fuel consumption in regime 1.

Value surfaces for the regime-switching case with respect to gas spot prices and boiler temperature for fixed electricity price are provided in Figure 14, while the corresponding surfaces with respect to electricity and gas spot prices are given in Figure 15. We can infer from these figures that the value surfaces are shifted down in regime 1 due to economic disruptions.

9 Conclusion

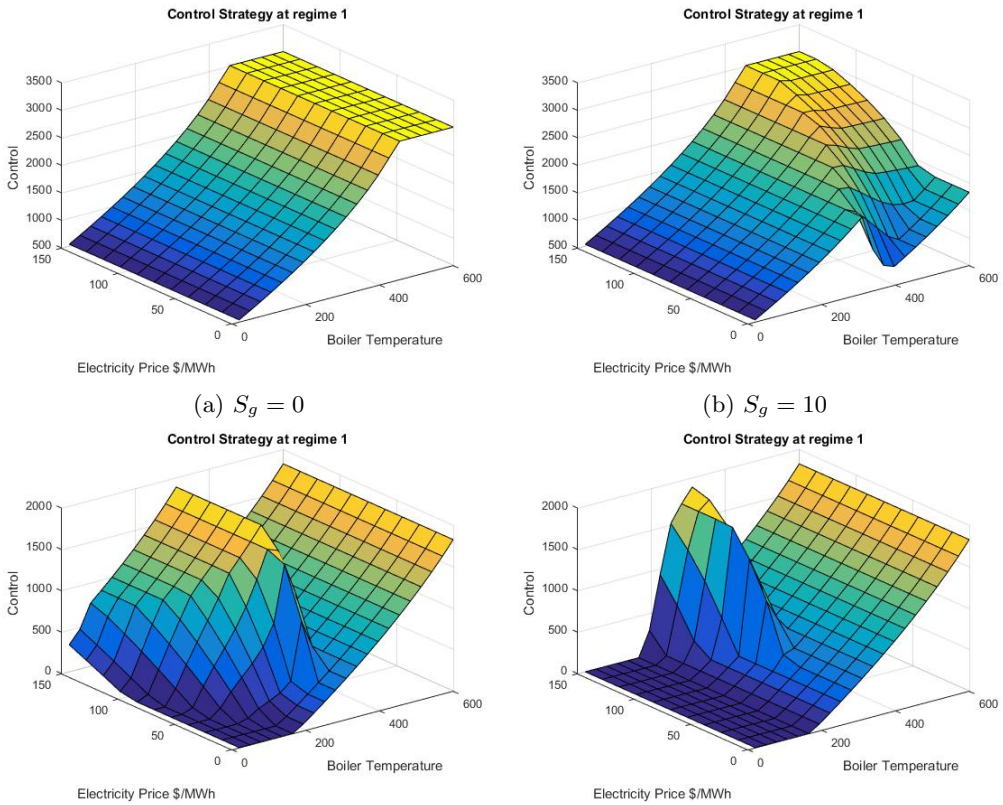
In this research we have analysed a stochastic control problem for gas-fired power generators while taking into account operating characteristics. The optimisation method introduced by Thompson et al. (2004) has been elaborated



(a) $S_g = 0$ (b) $S_g = 10$

(c) $S_g = 14$ (d) $S_g = 20$

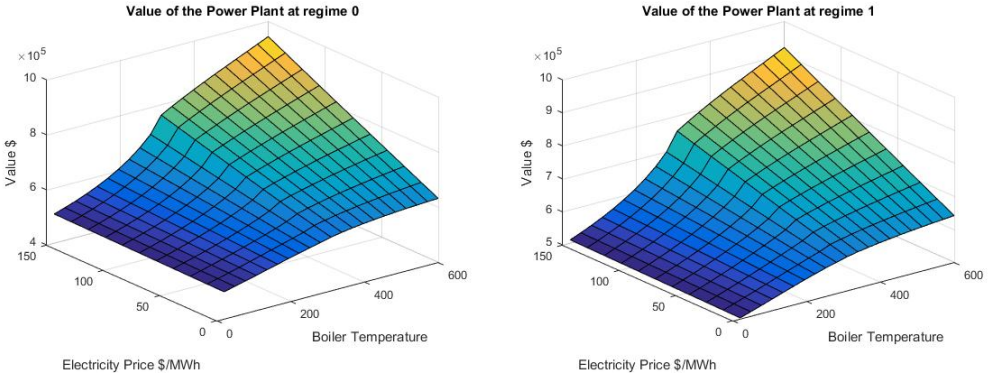
Figure 9: Operating strategy for the regime 0 of the regime-switching model with respect to electricity spot price and boiler temperature for different gas prices.



(a) $S_g = 0$ (b) $S_g = 10$

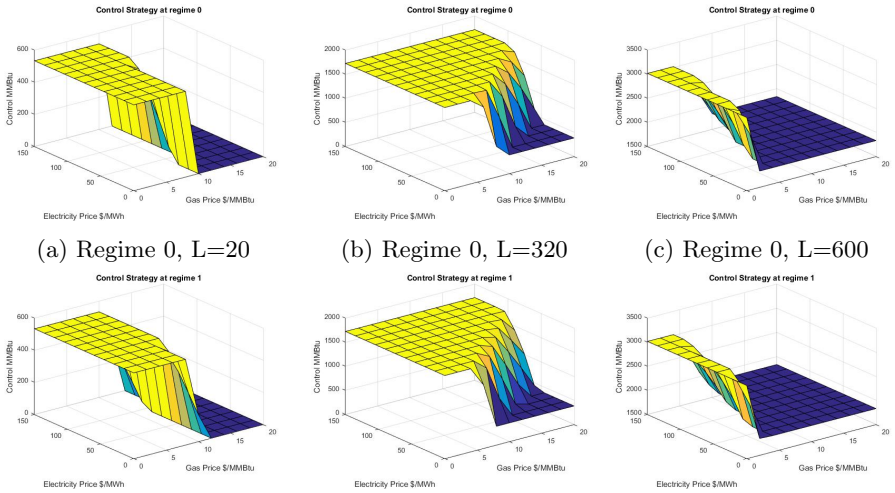
(c) $S_g = 14$ (d) $S_g = 20$

Figure 10: Operating strategy for the regime 1 of the regime-switching model with respect to electricity spot price and boiler temperature for different gas prices. Comparison with Figure 9 show that under both of these regimes the optimal strategy for $S_g \to 0$ is to burn maximum amount of gas all the time (a). For all other non-zero natural gas prices the maximum fuel consumption region is larger for the regime 0 than for the regime 1. When gas prices are too expensive the plant no longer consumes fuel when electricity prices are low and $L < 300°\text{C}$. Therefore, the optimal strategy surface becomes more pessimistic under the regime-switching model.



(a) Regime 0 (b) Regime 1

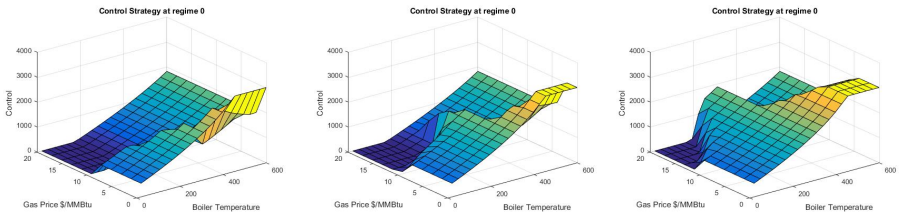
Figure 11: Value surfaces for the regime-switching model with respect to power prices and boiler temperature for fixed gas price. Although the surfaces look similar in their shapes, there is a downside shift in regime 1 which reflects an unfavorable economic situation.



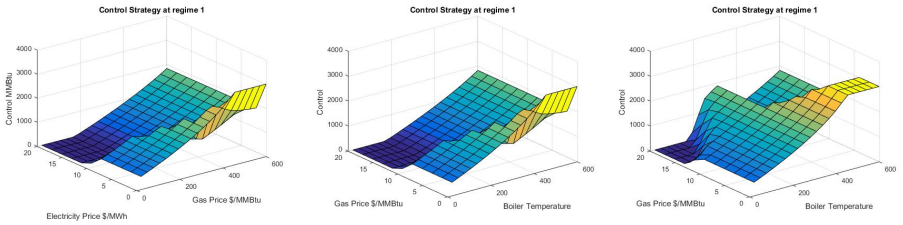
(a) Regime 0, L=20 (b) Regime 0, L=320 (c) Regime 0, L=600

(d) Regime 1, L=20 (e) Regime 1, L=320 (f) Regime 1, L=600

Figure 12: Operating strategy for regime-switching model with respect to electricity and gas spot prices for different boiler temperatures. Optimal operation surfaces are more risk-averse in regime 1 when the temperature is above the operating level $L = 300°\text{C}$. As the plant doesn't produce electricity below 300°C, the change in electricity prices does not affect our decision making. Hence, in regime 1 the optimal control surface for $L = 20°\text{C}$ is more optimistic than in regime 0 due to fall in gas spot prices ((a) and (d)). Moreover, in contrast to Figure 7, the surface isn't flat when the temperature is close to its minimum.

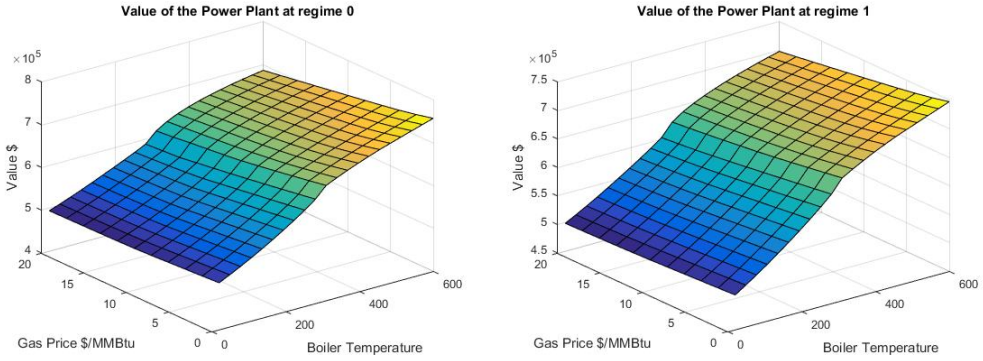


(a) Regime 0, $S_e = 0$ (b) Regime 0, $S_e = 60$ (c) Regime 0, $S_e = 150$



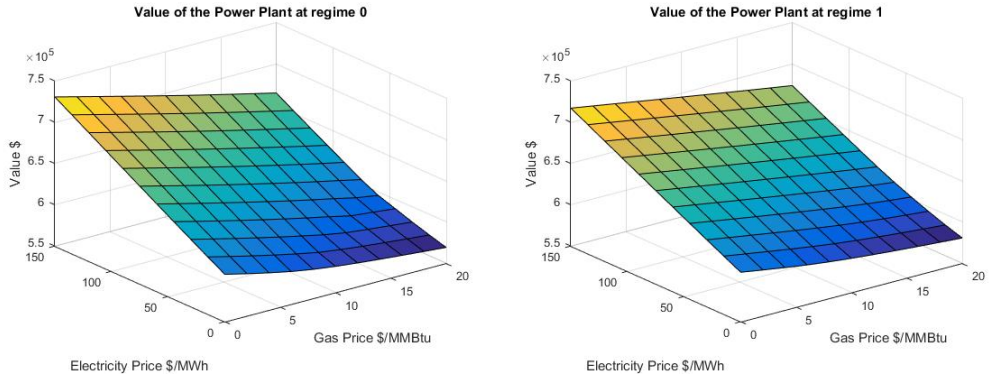
(d) Regime 1, $S_e = 0$ (e) Regime 1, $S_e = 60$ (f) Regime 1, $S_e = 150$

Figure 13: Operating strategy for regime-switching model with respect to gas spot prices and boiler temperature for different power prices. When the power prices For extremely low or high power prices the surfaces in regimes 0 and 1 look very similar. However, we have a larger region of minimal fuel consumption in regime 1 for moderate electricity prices.



(a) Regime 0 (b) Regime 1

Figure 14: Value surfaces for the regime-switching model with respect to gas spot prices and boiler temperature for fixed electricity price. The value surface is shifted down in regime 1 due to economic disruptions.



(a) Regime 0 (b) Regime 1

Figure 15: Value surfaces for the regime-switching model with respect to electricity and gas spot prices for fixed boiler temperature. Less favourable economic situation resulted in downward shift in regime 1.

by incorporating electricity and natural gas spot prices that exhibit regime-switching and interdependent spikes. The dependence of the price jumps has been modeled by means of skewed Lévy copulas. We have combined different numerical techniques to solve the resulting coupled non-linear HJB equations. We have also used a minmod slope limiter to eliminate numerical oscillations from the optimal solution. The numerical approach gives us both the value of the power plant and optimal control strategy depending on the electricity and gas price, boiler temperature and time. The numerical approach has been implemented in MATLAB for a single regime and regime-switching cases. We have investigated the differences in those models by observing the surfaces of optimal operation and value surfaces.

As the next step, we plan to extend our numerical examples to the cases when underlying power and natural gas spot prices follow interdependent generalised hyperbolic (see Eberlein 2001 and Eberlein & Prause 2002) and variance-gamma (see Madan et al. 1998 or Brody et al. 2012) Lévy models. The application of this optimisation approach into more complicated problem such as joint optimisation of gas storage and power plant facilities could also be investigated. Another generalisation could be the optimal control of a multi-fuel power generating asset. In this case carbon emission and transaction costs (see Atkinson & Mokkhavesa 2004) of each fuel should also be incorporated to the model.

References

Atkinson, C. & Mokkhavesa, S. (2004), 'Multi-asset portfolio optimization with transaction cost', *Applied Mathematical Finance* **11**(2), 95–123.

Barndorff-Nielsen, O. E. & Shephard, N. (2001), 'Non-Gaussian Ornstein–

Uhlenbeck-based models and some of their uses in financial economics', *Journal of the Royal Statistical Society: Series B (Statistical Methodology)* **63**(2), 167–241.

Benth, F. E. (2011), 'The stochastic volatility model of Barndorff-Nielsen and Shephard in commodity markets', *Mathematical Finance* **21**(4), 595–625.

Benth, F. E., Benth, J. S. & Koekebakker, S. (2008), *Stochastic modelling of electricity and related markets*, Vol. 11, Singapore: World Scientific.

Benth, F. E., Kallsen, J. & Meyer-Brandis, T. (2007), 'A non-Gaussian Ornstein–Uhlenbeck process for electricity spot price modeling and derivatives pricing', *Applied Mathematical Finance* **14**(2), 153–169.

Benth, F. E. & Kettler, P. C. (2011), 'Dynamic copula models for the spark spread', *Quantitative Finance* **11**(3), 407–421.

Benth, F. E., Vos, L. et al. (2013), 'Pricing of forwards and options in a multivariate non-Gaussian stochastic volatility model for energy markets', *Advances in Applied Probability* **45**(2), 572–594.

Bjerksund, P., Stensland, G. & Vagstad, F. (2008), 'Gas storage valuation: Price modelling v. optimization methods', *Optimization Methods. NHH Dept. of Finance and Management Science Discussion Paper* (2008/20).

Boogert, A. & De Jong, C. (2008), 'Gas storage valuation using a Monte Carlo method', *Journal of Derivatives* **15**(3), 81–98.

Boogert, A. & de Jong, C. (2011), 'Gas storage valuation using a multifactor price process', *Journal of Energy Markets* **4**(4), 29–52.

Brody, D. C., Hughston, L. P. & Mackie, E. (2012), 'General theory of geometric Lévy models for dynamic asset pricing', *Proc. Roy. Soc. Lond. A* **468**(2142), 1778–1798.

Carmona, R. & Ludkovski, M. (2010), 'Valuation of energy storage: An optimal switching approach', *Quantitative Finance* **10**(4), 359–374.

Chen, Z. & Forsyth, P. A. (2010), 'Implications of a regime-switching model on natural gas storage valuation and optimal operation', *Quantitative Finance* **10**(2), 159–176.

Cont, R. & Tankov, P. (2003), *Financial modelling with jump processes*, Boca Raton: CRC press.

Cont, R. & Voltchkova, E. (2005*a*), 'A finite difference scheme for option pricing in jump diffusion and exponential Lévy models', *SIAM Journal on Numerical Analysis* **43**(4), 1596–1626.

Cont, R. & Voltchkova, E. (2005*b*), 'Integro-differential equations for option prices in exponential Lévy models', *Finance and Stochastics* **9**(3), 299–325.

Davis, P. J. & Rabinowitz, P. (2007), *Methods of numerical integration*, New York: Dover Publications.

Deng, S.-J., Johnson, B. & Sogomonian, A. (2001), 'Exotic electricity options and the valuation of electricity generation and transmission assets', *Decision Support Systems* **30**(3), 383–392.

Deng, S.-J. & Oren, S. S. (2003), 'Incorporating operational characteristics and start-up costs in option-based valuation of power generation capacity', *Probability in the Engineering and Informational Sciences* **17**(02), 155–181.

Dixit, A. K. & Pindyck, R. S. (1994), *Investment under uncertainty*, Princeton: Princeton University Press.

Eberlein, E. (2001), *Application of Generalized Hyperbolic Lévy Motions to Finance*, Boston: Birkhäuser, pp. 319–336.

Eberlein, E. & Prause, K. (2002), The generalized hyperbolic model: financial derivatives and risk measures, *in* 'Mathematical Finance Bachelier Congress 2000', Springer, pp. 245–267.

Hamilton, J. D. (1990), 'Analysis of time series subject to changes in regime', *Journal of Econometrics* **45**(1), 39–70.

Henaff, P., Laachir, I. & Russo, F. (2013), 'Gas storage valuation and hedging: a quantification of the model risk', *arXiv:1312.3789* .

Jacod, J. & Shiryaev, A. (2013), *Limit theorems for stochastic processes*, Vol. 288, Berlin: Springer.

Kallsen, J. & Tankov, P. (2006), 'Characterization of dependence of multidimensional Lévy processes using Lévy copulas', *Journal of Multivariate Analysis* **97**(7), 1551–1572.

Kyprianou, A. (2006), *Introductory lectures on fluctuations of Lévy processes with applications*, Berlin: Springer.

LeVeque, R. J. (1992), *Numerical methods for conservation laws*, Vol. 132, Basel: Springer.

Longstaff, F. A. & Schwartz, E. S. (2001), 'Valuing American options by simulation: A simple least-squares approach', *Review of Financial studies* **14**(1), 113–147.

Madan, D. B., Carr, P. & Chang, E. C. (1998), 'The variance gamma process and option pricing', *European finance review* **2**(1), 79–105.

Meyer-Brandis, T. & Morgan, M. (2014), 'A dynamic Lévy copula model for the spark spread', *Quantitative Energy Finance* pp. 237–257.

Näsäkkälä, E. & Fleten, S.-E. (2005), 'Flexibility and technology choice in gas fired power plant investments', *Review of Financial Economics* **14**(3), 371–393.

Parsons, C. (2013), 'Quantifying natural gas storage optionality: a two-factor tree model', *Journal of Energy Markets* **6**(1), 95–124.

Pindyck, R. S. (1993), 'Investments of uncertain cost', *Journal of financial Economics* **34**(1), 53–76.

Reich, N., Schwab, C. & Winter, C. (2010), 'On Kolmogorov equations for anisotropic multivariate Lévy processes', *Finance and Stochastics* **14**(4), 527–567.

Safarov, N. & Atkinson, C. (2016), 'Natural gas storage valuation and optimization under time-inhomogeneous exponential Lévy processes', *International Journal of Computer Mathematics* pp. 1–19.

Schoutens, W. (2003), *Lévy Processes in Finance Pricing Financial Derivatives*, Chichester: John Wiley & Sons Ltd.

Schwartz, E. S. (1997), 'The stochastic behavior of commodity prices: Implications for valuation and hedging', *Journal of Finance* **52**(3), 923–973.

Takashima, R., Naito, Y., Kimura, H. & Madarame, H. (2007), 'Investment in electricity markets: equilibrium price and supply function', *11th Annual Real Options Conference, Berkeley* pp. 6–9.

Thompson, M., Davison, M. & Rasmussen, H. (2004), 'Valuation and optimal operation of electric power plants in competitive markets', *Operations Research* **52**(4), 546–562.

Thompson, M., Davison, M. & Rasmussen, H. (2009), 'Natural gas storage valuation and optimization: A real options application', *Naval Research Logistics (NRL)* **56**(3), 226–238.

Tseng, C.-L. & Barz, G. (2002), 'Short-term generation asset valuation: a real options approach', *Operations Research* **50**(2), 297–310.

Wood, A. J. & Wollenberg, B. F. (2012), *Power generation, operation, and control*, Hoboken NJ: John Wiley & Sons.